

Magnetic-PLGA nanohybrids as theranostics against cancer

M.Sc. Thesis

By

YOGESH



**DEPARTMENT OF BIOSCIENCES AND
BIOMEDICAL ENGINEERING**

**INDIAN INSTITUTE OF
TECHNOLOGY INDORE**

MAY, 2023

Magnetic-PLGA nanohybrids as theranostics against cancer

A THESIS

*Submitted in partial fulfillment of the
requirements for the award of the degree*

of

Master of Science

by

YOGESH



**DEPARTMENT OF BIOSCIENCES AND BIOMEDICAL
ENGINEERING**

**INDIAN INSTITUTE OF TECHNOLOGY
INDORE**

MAY, 2023

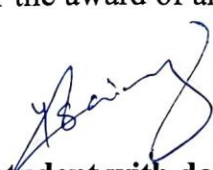


INDIAN INSTITUTE OF TECHNOLOGY INDORE

CANDIDATE'S DECLARATION

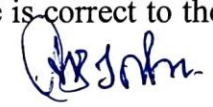
I hereby certify that the work which is being presented in the thesis entitled '**Magnetic-PLGA nanohybrids as theranostics against cancer**' in the partial fulfillment of the requirements for the award of the degree of **MASTER OF SCIENCE** and submitted in the **DEPARTMENT OF BIOSCIENCES AND BIOMEDICAL ENGINEERING**, Indian Institute of Technology Indore, is an authentic record of my own work carried out during the time period from September 2021 to May 2023 under the supervision of Dr. Abhijeet Joshi Associate Professor, Department of Biosciences and Biomedical Engineering.

The matter presented in this thesis has not been submitted by me for the award of any other degree of this or any other institute.


Signature of the student with date

Yogesh

This is to certify that the above statement made by the candidate is correct to the best of my/our knowledge.


Signature of Supervisor of M.Sc. Thesis with date

Dr. Abhijeet Joshi

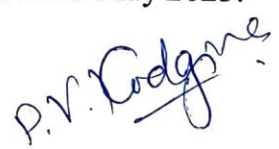
YOGESH has successfully given his/her M.Sc. Oral Examination held on 09 May 2023.


Signature(s) of Supervisor(s) of MSc thesis

Date:


Signature of PSPC Member #1

Date: 09.05.2023


Convener, DPGC

Date:


Signature of PSPC Member #2

Date: 17/5/2023

ACKNOWLEDGEMENTS

I commenced my journey here with almost zero prior knowledge or experience of working in any lab. This project would not get completed without the support of many members over here and for that I extend my honest gratitude towards each and every person who directly or indirectly taught me various things during this research project journey.

Firstly, I extend my gratitude towards my project instructor **Dr. Abhijeet Joshi** who never minded my silly mistakes and taught me every little thing required in any profession. In every meeting, he always promoted discussion on ideas whether about research or life. His calm and gentle nature is truly incredible by which I also learnt life long skills. This has been an epic journey for me working under his supreme guidance.

Dr. Sharan sir (NPDF) who treated me as his own little brother and taught every single thing from lab techniques, Excel to some sports skills. I extend my honest gratitude to him as without him I cannot even think to complete this project journey of my masters. **Badri Sahoo**(Ph.D.) with whom a bond of brotherhood I shared due to learning and teaching various lab skills and research ideas discussions. **Tanishq** who was always there to teach me enormous tech skills and supported at every step whenever I needed. I also extend my gratitude to every other lab member **Mr. Tanmay, Tileshwar, Jaspreet Kaur, Bhawana Joshi** to be there for every kind of support and guidance.

I would like to thank my PSPC members, **Prof. Avinash Sonawane** and **Dr. Kiran Bala**, for their valuable suggestions during the project's progress. I like to thank **Prof. Amit Kumar** (HOD, BSBE), **Prof. Prashant Kodgire** (DPGC convenor) and **s** (course coordinator). A very special thanks to **Prof. Amit Kumar** as it was him who encouraged & motivated me to go for whatever I aspired.

I am very grateful to **Prof. Amit Kumar** and **Dr. Hem Jha** and for providing the required cells lines timely.

I extend my gratitude to all faculty members of BSBE, IIT Indore, for demonstrating and teaching me new research techniques. I would like to thank **Prof. Suhas Joshi** (Director, IIT Indore) for allowing me to be a part of this eminent institute.

I want to thank the BSBE department (**Mr. Arif Patel, Mr. Gaurav Singh,** and **Mr. Murphy sir**) and SIC, IIT Indore, for the instrumentational facilities. unconditional love, support and care. A very special thanks to **Mrs. Mitali Dave** to teach me the operation of SEM at SIC and **Ravindra Kumar** sir for his supportive and kind nature at CLSM facility.

I also extend my humble gratitude towards **Mr. Kamaljeet Singh Paink** (PhD Physics) who gave his precious time to try to compile magnetic hyperthermia instrument. I also thank to **Mr. Praveen Kumar** (PhD Chemistry) and **Mr. Nitin Kumar** (PhD Chemistry) to teach me rota-evaporator and other lab facilities required. I also thank to **Mr. Dikeshwar** (PhD Physics) for his constant support and efforts in finding and compiling the hyperthermia instrument.

No words can do justice if I try to thank **my parents** for their supreme sacrifices, love, care, strength and devotion in my studies throughout my whole life. They have been the truest inspiration to me to achieve something in this little life to make them proud. Lastly **my siblings** whose constant support and encouragement fulfilled me with joy and positivity in every kind of situation.

Thanks to all to make this journey of experiments fruitful to me and a memorable chapter of my life.

*Dedicated to my parents
Sh. Dharamvir Singh,
Smt. Ritu and my
siblings.*

Abstract

Cancer has been a deadly disease so far with millions of deaths annually. There are enormous trails going on towards the prevention and cure of this disease, developing various kinds of therapies. Due to adverse side effects in all the current therapies of cancer, specifically with synthetic chemotherapeutic drugs, the current research is more towards phytochemicals due to their antioxidant, anti-inflammatory and anti-cancer properties. In the recent studies various phytochemicals have shown considerable cytotoxicity towards different kinds of cancer but they also face some problems with their poor solubility, specificity and bioavailability. In this case nanotechnology comes into effect which is proven for the various modification of the nanoparticles leading to more improved drug delivery. PLGA and MNP have been used since long for drug delivery leading to more sustained and specific drug bioavailability protecting from degradation to its target site. This thesis aims to investigate the use of piperine and camptothecin-loaded PLGA and MNP-based drug delivery systems for cancer therapy, with a focus on their mechanisms of action and potential clinical applications. The current state of cancer therapy, the properties and applications of the compounds and delivery systems, and their potential for cancer treatment will be discussed.

LIST OF PUBLICATIONS

- **From thesis:**

1. Piperine-loaded PLGA-magnetic nanohybrid as an effective theranostic against cancer (Manuscript under preparation)

- **Apart from thesis:**

1. **Singh, Y.**, Meena, T., V S, Sharan Rathnam, Vyas, T., Joshi, A., Sonawane, A. Emerging applications of nanotechnology in human welfare, 2022. (Manuscript submitted)
2. Shanmuga, S. R., Deepak, T., Sahoo, B., Meena T., **Singh, Y.**, and Joshi, A. Metallic nanocarriers for therapeutic peptides: Emerging solutions addressing the delivery challenges in brain ailments (Manuscript submitted)

TABLE OF CONTENTS

LIST OF FIGURES.....	xvii
LIST OF TABLES.....	xix
NOMENCLATURE.....	xxi
ACRONYMS.....	xxii
Chapter 1	1
Introduction and Literature Review	1
1.1 Introduction	1
1.2 Literature Review	3
1.2.1 Cancer	3
1.2.2 Current treatment strategies and associated issues	4
1.2.2.1 Surgical Methods	4
1.2.2.2 Chemotherapy	4
1.2.2.3 Radiation Therapy	5
1.2.2.4 Photodynamic Therapy	6
1.2.2.4 (a) Mechanism of Action and Challenges	6
1.3	9
Phytochemicals	9
1.3.1 Piperine	9
1.3.2 Mode of action	10
1.4 Camptothecin	12
1.4.1 Mode of action	13
1.4.2 Drawbacks	13
1.5 Nanotechnology in medicine	14
1.6 PLGA Nanoparticles	15
1.7 Magnetic NP	17
1.8 Objective and Scope	18
Chapter 2	19
Material and Methods	19
2.1 Materials	19
<u>n</u>2.1.1 Cell Lines:	19

2.1.2 Chemicals:	19
2.2 Methods	19
2.2.1 Synthesis of unloaded PLGA nanoparticles	19
2.2.2 Synthesis of Magnetic NPs	21
2.2.3 Synthesis of PF (PLGA-Fe₃O₄) nanoparticles	21
2.2.4 Synthesis of Pip-PLGA-Magnetic (PFP) Nanohybrid	22
2.2.5 Encapsulation efficiency	23
2.2.6 <i>In vitro</i> drug release study	24
2.2.7 Study of <i>In vitro</i> cytotoxicity through MTT assay	24
2.2.8 Estimation of ROS production and nuclear organization	25
2.2.9 Dual staining of GF-AFC and propidium iodide (PI) for the assessment of live/dead cell population	25
2.2.10 Dual staining of Calcein AM and propidium iodide (PI) for the assessment of live/dead cell population	26
Chapter 3	27
Results and Discussion of Applications of PFP	27
3.1 Preparation of UV-spectra of Piperine	27
3.2 Preparation of calibration curves of Pip	27
3.3 Characterization of MNP	28
3.3.1 Dynamic Light Scattering	28
3.3.2 Morphological analysis	29
3.3.3 Confirmation of functional groups	30
3.3.4 Crystal characterization by XRD	31
3.4 Characterization of PF:	32
3.5 Characterization of PFP	35
3.6 Encapsulation efficiency determination	37
3.7 <i>In vitro</i> Pip release study	39
3.8 Live-dead cell imaging through GF-AFC and PI staining	40
3.9 <i>In vitro</i> cytotoxicity assay	41
3.10 ROS production	43
3.10.1 Nuclear organization study	43
3.11 Live and dead imaging	46
3.12 Conclusion and future aspects	47

Chapter 4	49
Characterization and Application of PFC nanohybrids	49
4.1 Characterization of CPT:	49
4.2 Characterization of PFC nanohybrids:	50
4.3 Encapsulation efficiency calculation:	51
4.4 <i>In vitro</i> drug release	52
4.5 Conclusion and future aspects	53
APPENDIX	54
REFERENCES	59

LIST OF FIGURES

Figure 1.1: Structure of piperine.....	9
Figure 1. 2: Molecular mechanism of piperine inside cell showing how it leads to the activation of cascade pathway and further apoptosis. Also it can be seen that somehow it leads to ROS production which ultimately cause cell death. (Banerjee et al., 2021).....	11
Figure 1.3: Structure of Camptothecin	12
Figure 1. 4: Mechanism of CPT.....	13
Figure 1. 5: Physicochemical properties of PLGA NP that can be tuned with the surface modifications (adapted).....	16
Figure 3. 1: UV spectra of piperine showing their specific peaks at 344 nm in DMSO.....	27
Figure 3. 2: Calibration curve of pip in DMSO prepared at 344nm.....	28
Figure 3. 3: DLS analysis of magnetic NPs showcasing average size around 250nm with PI of 0.165 which tells about the uniformity of the NP in the solution form.....	29
Figure 3.4: FESEM images of MNPs showing spherical entities.....	30
Figure 3.5: The FTIR spectra of magnetic NP having characteristic stretches.....	31
Figure 3.6: XRD spectra of magnetic NP showing characteristic peaks.	32
Figure 3. 7: DLS analysis of PF nanohybrid showcasing average size around 137 nm with PI of 0.181 which tells about the uniformity of the NP in the solution form.....	33
Figure 3. 8: SEM images of PF nanohybrid showing uniformity in size and shape.....	34
Figure 3. 9: EDX spectra of PF single nanohybrid confirming the incorporation of PLGA-iron oxide nanoparticles. The spike of Fe can be seen in the figure in between 0 and 2 of x-axis.....	34

Figure 3. 10: The XRD spectra proving incorporation of PLGA and magnetic NPs.	35
Figure 3. 11: a) SEM images of PFP nanohybrid system. b) DLS analysis of nanohybrids.	36
Figure 3. 12: a) calibration curve of pip/DMSO prepared by using HPLC	38
Figure 3. 13: In vitro drug release study from PFP nanohybrids.....	39
Figure 3. 14: CLSM images of HT 29 cells stained with GF AFC and PI dyes showing live and dead cells in blue and red color respectively (A) for 48 h and. (B) for 72 h. V, pfv 50 ,100,200 and PFP 50, 100, 200 represents the concentration of PF and PFP in respective $\mu\text{g/ml}$. pip 50 represents concentration of pip in 50 $\mu\text{g/ml}$ taken as positive control.	41
Figure 3. 15: MTT results of (A) and (B) free pip on HT cells after 48 h and 72 h respectively. (C) MTT of treatment of PFP on HT 29 cells after 72 h.....	42
Figure 3. 16:- CLSM images of MDAMB 231 showing ROS & nuclear organization in green & blue color respectively. V 50, 100, 200 and PFP 50, 100, 200 represents the concentration of PF and PFP in respective $\mu\text{g/ml}$	44
Figure 3. 17: CLSM images of HT 29 cells showing ROS in green color. V 50, 100, 200 and PFP 50, 100, 200 represents the concentration of PF and PFP in respective $\mu\text{g/ml}$	45
Figure 3. 18: CLSM images of MDAMB 231 cells stained with calcein am and PI dyes showing live and dead cells in green and red color respectively. V 50 ,100,200 and PFP 50, 100, 200 represents the concentration of PF and PFP in respective $\mu\text{g/ml}$. pip 50 represents concentration of pip in 50 $\mu\text{g/ml}$ taken as positive control.....	46
Figure 4. 1: (a) UV spectra of CPT/DMSO (b) calibration curve	49
Figure 4. 3 : (a) : DLS analysis of PFC nanohybrids with PDI of 0.278.	50
Figure 4. 4: (b): FESEM images of PFC nanohybrids.....	51
Figure 4. 5: in vitro drug release of CPT out of PFC nanohybrids.....	52

LIST OF TABLES

Title	Page No.
Table 1. 1: The current statistics of cancer, causing death worldwide as per WHO	3
Table 1. 2: The various research studies on phyto-chemicals, PLGA, MNP NPs based drug delivery in cancer.....	8

NOMENCLATURE

Acronym	Expansion
CPT	Camptothecin
CLSM	Confocal laser scanning microscopy
DMSO	Dimethyl sulphoxide
DLS	Dynamic light scattering
EDX	Energy dispersive X-ray
FESEM	Field emission scanning electron microscopy
FTIR	Fourier transform Infrared
GF-AFC	Glycylphenylalanyl-aminofluoroumarin
HPLC	High performance liquid chromatography
MNP	Magnetic nanoparticles
MTT	(3-(4,5-dimethylthiazol-2-yl)-2,5-diphenyltetrazolium bromide dye)
NP	Nanoparticles
PF	PLGA- magnetic nanohybrids
PFC	CPT-PLGA-magnetic nanohybrids
PFP	Pip- PLGA-magnetic nanohybrids
PI	Propidium iodide
Pip	Piperine
PLGA	Poly (Lactide co-glycolide)
PVA	Polyvinyl alcohol
UV-vis	Ultraviolet visible
XRD	X-ray Diffraction

ACRONYMS

Sign	Meaning
λ	Wavelength
μ	Micron
$^{\circ}\text{C}$	Degree centigrade
$^{\circ}$	Degree
μl	Microliter
ml	Millilitre
L	Litre
nm	Nanometre
nM	Nanomolar
$\mu\text{g/ml}$	Microgram per millilitre
mbar	Millibar
s	Seconds
mins	Minutes
h	Hour
R^2	Regression coefficient

Chapter 1

Introduction and Literature Review

1.1 Introduction

Cancer remains the major global health problem and is responsible for approximately 9.6 million deaths in 2018, accounting for around one in six deaths worldwide (WHO, 2018). It is a complex disease characterized by uncontrolled cell growth that can invade and spread to other parts of the body. The development of cancer can be influenced by genetic mutations or exposure to carcinogenic agents, such as radiation, chemicals, and tobacco smoke (Blackadar, 2016). While treatment options such as surgery, chemotherapy, radiation therapy, and targeted therapy exist, they are often associated with adverse effects and may not be effective in all patients (Gharat et al., 2016). Phytochemicals are naturally occurring compounds found in plants that possess antioxidant, anti-inflammatory, and anticancer properties. They have shown promise in cancer prevention and treatment, as they can target various molecular pathways involved in cancer development and progression (Khan et al., 2022). Piperine, a phytochemical found in black pepper, has been shown to inhibit tumor growth, induce ROS (Reactive Oxygen Species) mediated apoptosis, and suppress metastasis, demonstrating its potential as an anticancer agent (Stojanović-Radić et al., 2019). Camptothecin, a natural compound, has been shown to induce ROS-mediated apoptosis and inhibit topoisomerase I, a crucial enzyme involved in DNA replication in S phase. Thus, it has been proved its potential against various cancers. The issue with these drugs remains their poor water solubility, poor bioavailability and low specificity.

In this regards encapsulation them with that of nanoparticles to enhance their impact has been tried in various studies & shown

remarkable results (Kaur et al., 2021). Poly(lactic-co-glycolic acid) (PLGA) is FDA approved completely biodegradable and biocompatible polymer which has been used in drug delivery systems. PLGA nanoparticles, in particular, are attractive as drug delivery vehicles for tumor therapy because of their ability to enhance drug solubility, protect drugs from degradation, and target tumors through the enhanced permeability and retention (EPR) effect (Mir et al., 2017). MNP (Magnetic Nanoparticles) possess unique magnetic properties that make them an attractive option for targeted drug delivery (Joshi and Joshi, 2022). They can be directed to specific tissues using magnetic fields and can enhance drug uptake by cells through magnetic guidance and also can be used as potential contrast enhancer in magnetic resonance imaging (MRI) (Mohapatra et al., 2023). MNPs have been explored as drug delivery vehicles for cancer therapy and have shown promising results. By combining phytochemicals, such as piperine, CPT and drug delivery systems, such as PLGA and magnetic NPs, the efficacy of cancer therapy can be improved while reducing adverse effects.

This thesis aims to explore the use of piperine and camptothecin-loaded PLGA and magnetic NP-based drug delivery systems for cancer therapy, with an emphasis on their mechanisms of action and potential clinical applications. The subsequent sections will discuss the current state of cancer therapy, the properties and applications of piperine, camptothecin, PLGA, and magnetic NPs in drug delivery systems, and the potential of these systems for cancer therapy.

1.2 Literature Review

1.2.1 Cancer

Cancer is a set of disorders that are identified by the unregulated proliferation and metastasis of abnormal cells within the body. In contrast, healthy cells within the body undergo cell division and growth in an organized manner, which is due to a property of normal cells that is contact inhibition but cancer cells divide and grow uncontrollably due to the loss of this property leading to the formation of a mass of tissue called a tumor. Cancer can arise in any part of the body and can spread to other parts through the bloodstream or lymphatic system. The process of cancer spread is called metastasis. Metastasis is one of the deadliest properties of cancer as it leads to the development of secondary tumors in different parts of the body. According to various estimates, the worldwide incidence of cancer has increased up to 18.1 million new cases and around 9.6 million deaths in 2018 alone. It is reported that one out of every five men and one out of every six women globally develop cancer at some point in their lives.

Table 1.1: The current statistics of cancer, causing death worldwide as per WHO

Cancer Type	Number of New Cases (2018)	% of Total Cancer Incidence	Number of Deaths (2018)	% of Total Cancer Deaths
Lung	2.1 million	11.6%	1.8 million	18.4%
Female Breast	2.1 million	11.6%	627,000	6.6%
Colorectal	1.8 million	10.2%	881,000	9.2%
Prostate	1.3 million	7.1%	-	-
Stomach	1.0 million	5.7%	783,000	8.2%
Liver	-	-	782,000	8.2%

lives, with one out of every eight men and one out of every eleven women dying from the disease. Additionally, the 5-year prevalence, which refers to the total number of individuals alive within five years of a cancer diagnosis worldwide, is estimated to be 43.8 million. The estimates and reported cases of the prevalent cancer cases in 2018 by WHO worldwide are figured out in Table 1.1 (WHO, 2018).

1.2.2 Current treatment strategies and associated issues

Based on the type and stage of cancer there are various treatment strategies available surgery, chemotherapy, radiation therapy, targeted therapy, and immunotherapy.

1.2.2.1 Surgical Methods

Surgery is a common method of cancer treatment that involves removing the cancerous tumor and surrounding tissues from the body. Surgery can be a highly effective method of cancer treatment, particularly when the cancer is localized and is static to that particular part only. However, surgery can also be associated with risks and potential complications, such as bleeding, infection, or damage to nearby organs or tissues.

1.2.2.2 Chemotherapy

Cancer chemoimmunotherapy has emerged as a promising strategy for enhancing the effectiveness of cancer treatment and has been extensively investigated in both preclinical and clinical studies. Chemotherapy is a commonly used cancer therapy that offers a ray of hope for cancer patients. This treatment works by utilizing toxic agents that inhibit the rapid growth and proliferation of cancer cells. However, this approach also has some drawbacks as it may inhibit the growth of other fast-growing cells in the body such as bone marrow cells, hair follicles and gastrointestinal tract cells, leading to several toxic side effects like severe nausea, hair loss and bowel problems. Furthermore, the success

rate of chemotherapy is often limited by issues like poor pharmacokinetics, wide distribution in vivo, non-specific delivery, and multiple drug resistance (MDR) (Zhang et al., 2017).

In the present times, the combination therapy approach has emerged as an enhanced curative approach along with surgery, radiation therapy, photothermal therapy and others (Mu et al., 2020).

1.2.2.3 Radiation Therapy

Radiation therapy is a commonly used cancer treatment that utilizes high-energy radiation to destroy cancer cells. As per various studies radiation therapy has demonstrated effectiveness in treating various types of cancer, including breast, prostate, lung, and head and neck cancers. A linear accelerator is typically used to administer this treatment, which delivers high-energy X-rays or electrons to the cancer site, causing damage to the cancer cell's DNA and inhibiting its ability to grow and divide (Baumann et al., 2016).

Radiation therapy can be administered alone or in combination with other treatments, such as chemotherapy and surgery, depending on the type and stage of cancer. Internal radiation therapy may involve the use of radioactive implants or injections to directly target cancer cells. It is essential to carefully evaluate the patient's condition and determine the appropriate radiation dosage to minimize the risk of side effects while maximizing the treatment's efficacy. However, radiation therapy can also cause some side effects, such as fatigue, skin irritation, and gastrointestinal issues. Therefore, it is crucial to take into account the potential risks and benefits of this treatment for each patient's specific case.

1.2.2.4 Photodynamic Therapy

Photodynamic therapy (PDT) is a promising and emerging treatment strategy for tumor that involves the use of photosensitizing agents, light, and oxygen to selectively destroy cancerous cells. The process of PDT involves the administration of a photosensitizer, which is then activated with a specific wavelength radiation to produce reactive oxygen species (ROS) that can cause cell death (Dougherty et al., 1998). While PDT has been studied for several decades, recent advancements in imaging technology, light sources, and photosensitizers have significantly improved its effectiveness as a cancer treatment. PDT has been shown to be effective in the treatment of various types of cancer, including skin, lung, esophageal, and bladder cancer (Dougherty et al., 1998). One of the recent advancements in PDT is the development of new photosensitizers with improved efficacy and specificity. For example, nanoparticles such as gold and silica can be loaded with photosensitizers and targeted to specific cancer cells or tissues, improving their selectivity and efficacy. Another recent development in PDT is the use of combination therapies. PDT can be combined with other therapies such as chemotherapy, radiation therapy, and immunotherapy to improve treatment outcomes (Josefsen and Boyle, 2008).

1.2.2.4 (a) Mechanism of Action and Challenges

The mechanism of PDT involves the use of a photosensitizer that is selectively taken up by cancerous cells. Once the photosensitizer is activated with a specific wavelength, it produces ROS, such as singlet oxygen, which can damage cellular components and lead to cell death (Castano et al., 2004). Despite the potential benefits of PDT, there are several challenges and limitations to its use. One of the main limitations is the depth of tissue penetration, as the effectiveness of PDT decreases with increasing tissue depth (Henderson and Dougherty, 1992). Additionally,

PDT can cause photosensitivity, which can limit patient mobility and require special precautions (Gharat et al., 2016). Furthermore, the cost of PDT is often higher than other cancer treatments, which can be a barrier to its widespread use.

We went through various literature articles for finding the ongoing treatment strategies for such deadly disease. Some of them are listed in the Table 1.2 below showing the role of natural compounds as an alternate of synthetic compounds which causes various adverse side effects and other health problems discussed above. In the recent times, the role of nanotechnology in medicines has emerged as fruitful solution to enhance overall drug efficacy in various kinds of treatments leading to fewer side-effects and enhanced bioavailability of enormous compounds whether these are natural or synthetic.

Table 1. 2: The various research studies on phyto-chemicals, PLGA, MNP NPs based drug delivery in cancer.

Author(s)	Drug and Carrier	Objective
(Kaur et al., 2021)	Piperine – loaded PLGA	To test efficiency of PLGA as cancer drug carriers
(Banerjee et al., 2021)	Piperine	To observe anticancer effects in leukemia cell line
(Jabalera et al., 2019)	PLGA	To check cytotoxic effect of PLGA-loaded DOXO with magnetic hyperthermia and photothermia
(Khan et al., 2022)	Natural compounds	Role of phytochemicals in Cancer Treatment and Their Mechanisms of Action
(Bao et al., 2019)	Camptothecin	The impact of camptothecin-encapsulated poly(lactic-co-glycolic acid) nanoparticles on the activity of cytochrome P450 in vitro
(Almeida et al., 2022)	Chitosan and Camptothecin	Oral delivery of camptothecin-loaded multifunctional chitosan-based micelles is effective in reduce colorectal cancer
(Jannah and Onggo, 2019)	Fe ₃ O ₄ NPs	Synthesis of MNP
Pablo Guardia et al.	Iron oxide nanocubes	To observe the increased efficacy of magnetic NPs via hyperthermia in KB cells
(Mir et al., 2017)	Review	Recent applications of PLGA based nanostructures in drug delivery

1.3 Phytochemicals

There has been a very fast progress for prevention and treatment of cancer, but still huge gaps exist demanding multiple improvements. The modern synthetic chemotherapeutic drugs and even other curing methods which are in use in the present times causing various side effects and serious health issues. Since long plant-based drugs/compounds have been used in treatment of various diseases. Many Researches have confirmed the effectiveness of these plant-based medications leading to the discovery and development of these natural compounds. These phytochemicals are generally secondary metabolites (Catalano, 2016) used in various applications having considerable therapeutic potential along with very few side effects in lower costs (Khan et al., 2022). Consuming a diet high in fruits and vegetables, which are rich in phytochemicals, has been associated with a reduced risk of several types of cancer. Despite this, a significant proportion of cancer-related deaths could be prevented by adopting a "healthy" lifestyle, including proper nutrition. Various phytochemicals, such as carotenoids, antioxidants, phenolic compounds, terpenoids, steroids, indoles, and fibers, are believed to contribute to this risk reduction (Catalano, 2016).

1.3.1 Piperine

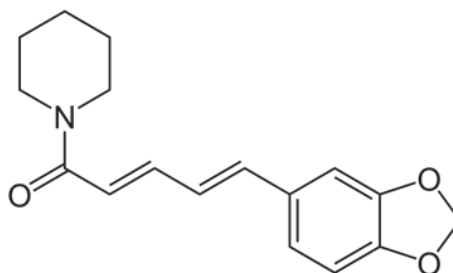


Figure 1.1: Structure of piperine

Piperine, which imparts the characteristic pungent taste to black pepper (*Piper nigrum L.*), is the primary bioactive constituent present in it. Chemically it belongs to alkaloid category. Pepper has been widely used as a culinary spice in numerous countries, but it has also been traditionally employed as a medicinal herb. According to Ayurvedic medicine, pepper is a constituent of 'trikatu,' which includes long pepper, black pepper and ginger in equal amounts, and is the foundation for 210 of the 370 remedies listed in the Handbook of Domestic Medicine and Common Ayurvedic Remedies. Traditionally, piperine has been used to cure various diseases like gastrointestinal conditions, asthma, bronchitis, fever. In Chinese medicine also, piperine has been vastly used to cure headaches, muscular pain, rheumatism, throat infection and for enhancing blood flow as well (Stojanović-Radić et al., 2019). Piperine shows higher permeation rate due to its lipophilic nature and non-saturable absorption kinetics. And also it has been seen inhibiting p-glycoprotein efflux leading to enhanced penetration of other drug molecules along with it (Chaudhari et al., 2021). There are various articles providing the information about the anti-cancerous properties of piperine inhibiting the further proliferation of tumor i.e. piperine inhibited tumor proliferation due to activation of caspase-3, ROS production leading to cellular apoptosis in KB cells (Siddiqui et al., 2017), free pip and chitosan coated liposomes showed inhibitory effect on MCF7 cells proliferation (Imam et al., 2021).

1.3.2 Mode of action

It exerts its anti-tumor effects through various mechanisms, such as induction of cell cycle arrest, apoptosis, and inhibition of angiogenesis. Piperine has been found to increase the expression of pro-apoptotic proteins, such as Bax and caspase-3, while diminishing the expression of

Bcl-2 like anti-apoptotic proteins. Briefly piperine after entering to the cell inhibits the Bcl-2 (antiapoptotic protein) activating further the apoptotic gene Bax due to which Cyt C comes out of the mitochondrial membrane leading to the activation of caspase activity which further activate the caspase 3 and caspase 9 leading to apoptosis of the cells. Also piperine leads to ROS production which ultimately lead to cell death(Banerjee et al., 2021). One of the major limitations of free drugs is their lower water solubility, which can lead to difficulties in their delivery and efficacy.

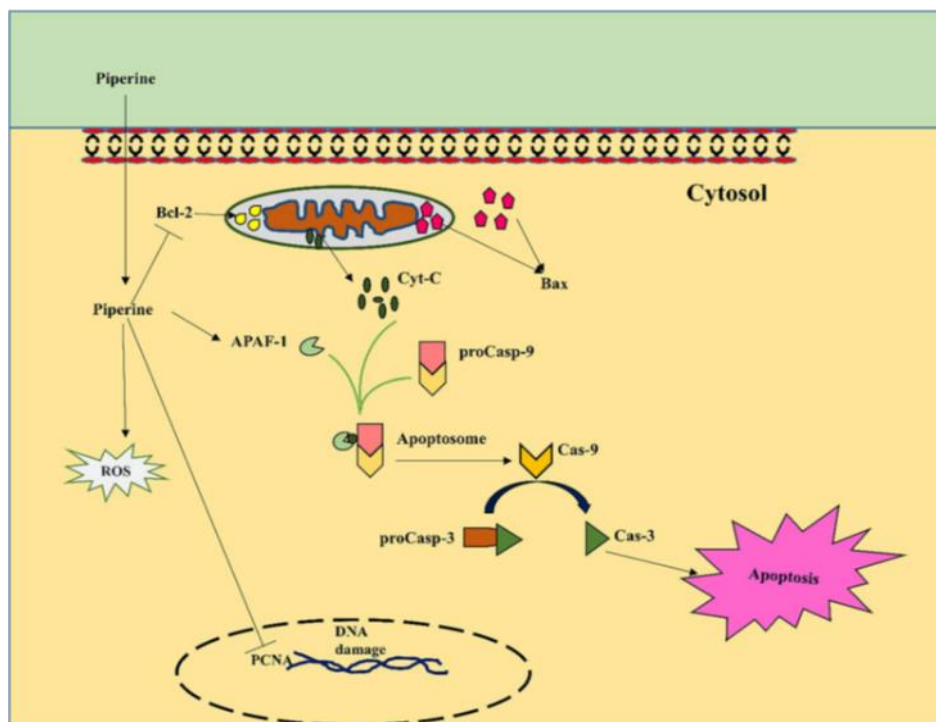


Figure 1. 2: Molecular mechanism of piperine inside cell showing how it leads to the activation of cascade pathway and further apoptosis. Also it can be seen that somehow it leads to ROS production which ultimately cause cell death. (Banerjee et al., 2021).

Additionally, they may have poor bioavailability and pharmacokinetics, meaning that they may not be efficiently absorbed and distributed throughout the body. Another limitation is poor photostability, which can cause isomerization when exposed to UV rays, resulting in

changes to the drug's structure and potentially reducing its effectiveness. (Salsabila et al., 2021).

1.4 Camptothecin

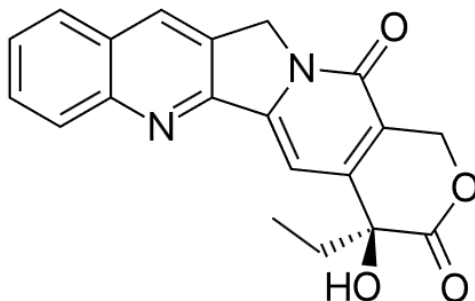


Figure 1.3: Structure of Camptothecin

Camptothecins have emerged as crucial alkaloids for combating cancer in the 21st century, as their clinical applications testify. In 1966, Wall and Wani discovered and purified 20-(S)-Camptothecin (CPT) during a plant screening aimed at identifying novel steroids, from the bark of *Camptotheca acuminata Decne.*, commonly known as the Chinese Happy Tree (Martino et al., 2017). Structurally and chemically, it is a quinoline alkaloid compound. It has been tested and showed positive results when given to the various cancer cell lines i.e. When treated to HCT 116 colon cancer cell line, it showed tremendous cytotoxicity (in free as well as loaded in chitosan NP) to the cells even at very low concentrations (nM) (Almeida et al., 2022), it inhibited the metastatic proliferation of breast cancer when applied using with silicon NPs in MDAMB-231 cell lines (Landgraf et al., 2020), when applied to HepG2 cells, in free as well as loaded in PLGA NP CPT showed considerable cytotoxicity inhibiting the further cellular proliferation (Bao et al., 2019).

1.4.1 Mode of action

CPT is known to be the poison of DNA Top 1 enzyme which is very crucial in cellular information flow machinery like replication, transcription, various recombination and repair processes (Martino et al., 2017). The anticancer properties of CPTs rely on the creation of a non-covalent bond between CPT and the covalent binary complex generated by DNA and TOP 1. Typically, the equilibrium between free TOP I and the TOP I-DNA complex favors the unbound enzyme. While, in the presence of CPT, the equilibrium quickly shifts towards the formation of ternary complex, leading to the inhibition of TOP 1. The consistent presence of the ternary complex during DNA replication procedures results in alterations to the DNA sequence, which ultimately lead to cell death in CPT-treated cells (Pizzolato and Saltz, 2003).

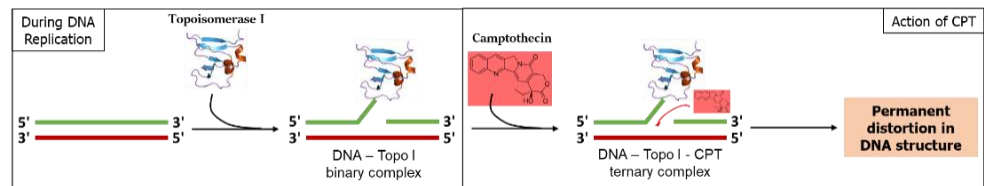


Figure 1. 4: Mechanism of CPT

1.4.2 Drawbacks

CPT failed due its dose limiting toxicities, poor efficacy (Bao et al., 2019) Its very poor water solubility, bioavailability and lower stability leads to limited use of this much potent drug molecule to a few (McCarron et al., 2008). Another major concern with its activity is when in its lactone form, CPT displays high activity, but under physiological conditions, it readily converts to a less active carboxylate form. This conversion leads to rapid clearance after binding with plasma proteins and elevated side effects (Hertzberg et al., 1989).

1.5 Nanotechnology in medicine

In 1959, Richard Feynman, an American physicist, and Nobel Prize laureate, introduced this new concept of nanotechnology. He delivered a lecture titled "There's Plenty of Room at the Bottom" during the annual meeting of the American Physical Society at the California Institute of Technology (Caltech). During this lecture, Feynman proposed a hypothesis that questioned the limits of miniaturization: "Why can't we condense the entire 24 volumes of the Encyclopedia Britannica onto the head of a pin?" He also described his vision of using machines to build progressively smaller machines, ultimately achieving molecular-scale construction (Bayda, et al., 2019). Over the last seventy years, research in this field has yielded remarkable outcomes in enhancing long-term care for various diseases, leading to an increase in life expectancy. However, translating and implementing drug delivery systems from the clinical stage to the product level requires deliberate efforts. Drug formulations, including tablets, ointments, capsules, and solution phases, have evolved over time to incorporate controlled-release formulations. Several recent studies have underscored the vast potential of nanotechnologies in the field of biomedicine, particularly for diagnosing and treating a range of human diseases.

Bio-nanotechnology is widely regarded as one of the most captivating areas of study in the field of nanoscience due to its ability to address the crucial issue of drug bioavailability at the desired site of action, which is influenced by the delivery approach employed. Although the pharmacokinetic and dynamic profile of a therapeutic agent is important, successful medical therapy relies heavily on its ability to achieve the desired outcomes through effective delivery (Mir et al., 2017). Achieving controlled release of toxic drugs exclusively at target sites can result in fewer side effects, lower doses, improved compliance, and ultimately, enhanced quality of life for patients. Over the past few decades, researchers have intensively studied and achieved excellent

results in the use of nanotechnology in various biology-related areas, including diagnosis, drug delivery, and molecular imaging. Significant advancements have also been achieved in the field of nano-oncology, specifically in enhancing the effectiveness of conventional chemotherapy drugs for various aggressive human cancers. This progress has been made possible by utilizing functional molecules such as nanoparticles, antibodies, and cytotoxic agents that target the tumor site (Yan Lee and K.Y. Wong, 2011). A diverse array of submicron materials has been developed and designed to combat cancer. These materials have facilitated the development of contrast agents, therapeutics, drug delivery vehicles, and theranostics. For drug delivery purposes, nanoparticles (NPs) have been created using biodegradable and biocompatible polymers derived from natural and/or synthetic materials. Both naturally derived and synthetic polymers, such as polysaccharides, polycaprolactone (PCL), poly(lactic acid) (PLA), poly(glycolic acid) (PGA), and polyethylene glycol (PEG), are suitable biomaterials for producing polymeric nanoparticles using techniques such as nanoprecipitation, emulsification, and self-assembly.(Zhang et al., 2020).

1.6 PLGA Nanoparticles

PLGA (Poly (D,L-lactide-co-glycolide)) is a type of synthetic polymer having monomers in the ratio of 1:1 that is both biodegradable and biocompatible. It has been approved by FDA (U.S Food and Drug Administration) and EMA (European Medical Agency) and is used in drug delivery technology. This polymer is particularly useful in nanomedicine because it has minimal systemic toxicity and breaks down into biodegradable metabolite monomers (lactic acid and glycolic acid) that are consumed in metabolic pathways such as the TCA (Krebs') cycle(Kaur et al., 2021). PLGA is able to deliver drug-loaded nanoparticles intravenously, allowing for controlled release and site-specific targeting. It is used to prepare a desired dosage form of drugs to

maintain an appropriate drug concentration in the bloodstream, resulting in a controlled release profile.

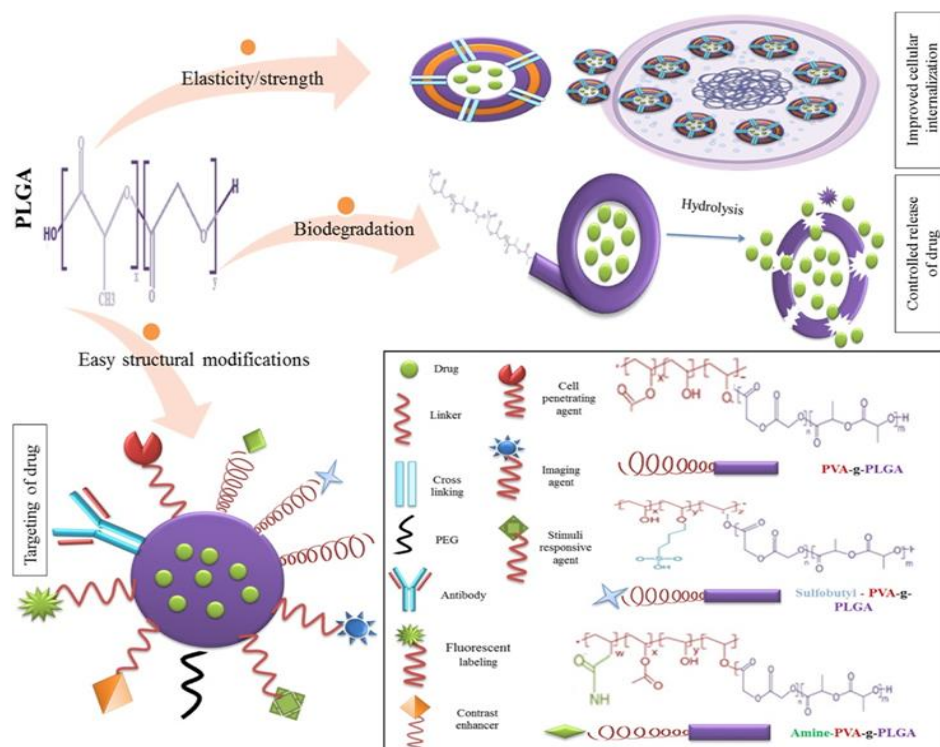


Figure 1. 5: Physicochemical properties of PLGA NP that can be tuned with the surface modifications (adapted from Mir et al., 2017).

PLGA nanoparticles can incorporate various types of drugs, including hydrophobic and hydrophilic molecules, vaccines, proteins, and biological components, either through encapsulation or surface conjugation that can be seen in the figure 1.4 (Mir et al., 2017). Nano-encapsulation facilitates cell entry, protects against early degradation, enhances solubility, and can even facilitate crossing the blood-brain barrier (BBB) (Yasaswi et al., 2021). The surface modification of PLGA NPs is crucial in determining their targeting strategy, biocompatibility, and blood half-life, in addition to their intrinsic properties. Combining PLGA with other polymers, such as polyethylene glycol (PEG), polyvinyl alcohol (PVA), and d- α -tocopheryl PEG 1000 succinate (TPGS), can increase their blood

half-life, among other benefits. PEGylation, which is a surface modification technique using PEG, enhances the hydrophilicity of the formulation, resulting in a stealth particle that has improved pharmacokinetics and longer blood circulation time. This is achieved by providing protection from opsonization and intake by various phagocytic cells (Rezvantalab et al., 2018).

1.7 Magnetic NP

In the recent times magnetic NPs (Fe_3O_4 : -Iron oxide NP) have been emerged as a great tool in drug delivery due to their various properties. To prevent agglomeration, these are coated with biodegradable compounds. Moreover, they can be conjugated with various targeting moieties to enable site-specific drug delivery (Palanisamy and Wang, 2019). Specifically magnetic NPs have been designed and used in cancer therapeutics due to their unique properties. One important characteristic is stability, as they must remain intact in physiological environments. They also need to be biocompatible and non-toxic to cells to avoid any potential harm. Another significant property is biodegradability, as they can be metabolized and utilized as iron stores for RBCs and hemoglobin formation. MNP are also relatively easy to synthesize, using methods such as hydrothermal or coprecipitation (Joshi and Joshi, 2022). Additionally, they have numerous applications in healthcare, such as bio-magnetic separation, magnetic hyperthermia, and bioimaging, where they act as a contrasting agent enhancer in magnetic resonance imaging (MRI) (Ibarra et al., 2015) . These emerging technologies have the potential to be a promising approach for curing tumor-like diseases, making MNP an exciting area of research in the biomedical field.

1.8 Objective and Scope

The objective of the thesis is to synthesize and evaluate nano-hybrid carriers for controlled drug delivery, with the aim of providing sustained and controlled release of therapeutic molecules against cancer cell lines. The thesis also aims to evaluate the benefits of dual-purpose using PF nanohybrids as a theranostic approach for bioimaging and therapeutic both.

The main focus points of this thesis are:

1. Synthesis of PF nanohybrids using ultrasonic atomizer and further encapsulating with drug molecules.
2. Characterization of morphology of these nanohybrids with various techniques.
3. Evaluation of *in vitro* drug release to obtain controlled and sustained drug release at physiological pH.
4. Exploring the efficacy of synthesized nanohybrids as anticancer drug carriers on *in vitro* cellular studies minimizing cytotoxicity further enhancing their therapeutic efficacy along with acting as a suitable contrasting agent for bioimaging through MRI.

Chapter 2

Material and Methods

2.1 Materials

2.1.1 Cell Lines: HT 29, MDAMB 231

2.1.2 Chemicals: Poly (D, L-lactide-co-glycolic acid) (PLGA) (1:1) (MW = 30 000–60 000), poly (vinyl alcohol) (PVA) (MW = 30 000–70 000), piperine (Pip.), and camptothecin(CPT) were purchased from Sigma Aldrich, India. FeCl₃ and FeSO₄ were bought from RANKEM Chemicals. Dimethyl sulphoxide (DMSO) and Acetone (HPLC grade, 97%) were bought from LOBA chemicals. Dulbecco's Modified Eagle Media (DMEM), Fetal Bovine Serum (FBS), Antibiotic/antimycotic, Trypsin-EDTA solution, Dulbecco's phosphate buffered saline (DPBS) and 3-(4,5-dimethylthiazol-2-yl)-2,5 diphenyltetrazolium bromide dye (MTT), were procured from Himedia. Human colorectal carcinoma (HT 29 cells) was kindly gifted by the Infection Bioengineering Lab and MDAMB 231 was kind gift from Dr Amit Kumar lab, Department of Biosciences and Biomedical Engineering at IIT Indore. GF-AFC (glycylphenylalanyl-aminofluoroumarin) was purchased from Promega. Propidium Iodide and calcein am was purchased from Thermofisher, India.

2.2 Methods

2.2.1 Synthesis of unloaded PLGA nanoparticles

PLGA nanoparticles were synthesized by Ultrasonic atomizer following modified emulsification and solvent evaporation method using an ultrasonic atomizer is a simple and reproducible method for preparing

polymeric nano/hybrid carriers. It is also a cost-effective and innovative technique for producing nanoparticles. This approach utilizes ultrasound resonance and vibration to generate fine particles at room temperature without any additional side effects. Compared to traditional methods that require multiple steps, the ultrasonic atomizer can incorporate drugs into polymeric carriers in a single step. Additionally, this technique employs a spraying method that enables continuous particle production, making it more commercially and industrially relevant than batch processes. By using an atomizer, drug-containing polymeric nano/hybrid carriers can be efficiently prepared and controlled in terms of particle size, drug loading efficiency, dispersity, and drug release behavior. In this PLGA dissolved in Acetone sprayed in PVA worked as a surfactant which further stabilizes the droplets. 0.5% (w/v) PLGA dissolved in acetone (organic phase) total volume 2ml and then we sprayed it using a syringe pump (Multi-Phaser, NE-300, New Era Pump Systems, NY) keeping flow rate at 0.3 ml/min and ultrasonic atomizer (Sonozap, 2005) power, the frequency at 3.5Watt, 130kHz respectively. The droplets of PLGA were sprayed into 1% PVA(50ml) acting as an aqueous phase and left for magnetic stirring at 1500 rpm. After completion of spraying, the residual acetone was evaporated by heating at 50-55°C for 10-15min on a magnetic stirrer under 300-400rpm. Then this formulation was centrifuged using ultracentrifuge (Optima XPN-80 Beckmann Coulter, Inc.) at 70000-80000g for a 25-30 min cycle and further washing was done with the distilled water three times in a row. Then after washing the pellet was lyophilized for further drying up overnight until it becomes dry completely. The dried NPs were then kept at 4°C for further analysis and characterization (Kaur et al., 2021).

2.2.2 Synthesis of Magnetic NPs

These were synthesized by coprecipitation method by taking FeCl_3 (1%) 120 ml mixed with FeSO_4 (1%) 60 ml in a 2:1 ratio. After mixing it was kept in a magnetic stirrer at 500-700 RPM and then 5M NaOH was poured into it drop by drop to maintain its pH at 12.0 keeping it on a magnetic stirrer. Then maintaining its pH at 12.0 it was kept on a Magnetic stirrer at 80-90 °C for about 2 hs. The solution was then centrifuged (Kubota centrifuge) at 3500 rpm for 15 min and it was washed thrice with absolute ethanol during centrifuging. After washing, the pellet was kept for further getting da dried in a microwave oven at 55 °C overnight to get dried completely. After getting dried, it was crushed and converted into powder form and stored for further analysis (Joshi and Joshi, 2022).

2.2.3 Synthesis of PF (PLGA- Fe_3O_4) nanoparticles

PF nanoparticles were prepared using ultrasonic atomization, a modified emulsification solvent evaporation method. This approach offers advantages over conventional methods, such as batch-to-batch consistency and scalability. The resulting nanoparticles exhibit a more uniform distribution of small-sized particles, making it a feasible option for large-scale production without the need for filtration or centrifugation methods because the nozzle of ultrasonic atomizer works on a combination of resonance and vibrational energy generated by the atomizer due to which it gets able to produce very fine nano or micro sized particles in a very controlled manner enhancing the overall efficacy.

PF nanoparticles were synthesized by Ultrasonic atomizer by above mentioned method in which PLGA dissolved in Acetone sprayed in PVA worked as a surfactant which further stabilizes the droplets. 20 mg of PLGA was dissolved in acetone making the organic phase, and 50 ml of 1% PVA with 5mg ferrite nanoparticles made the aqueous phase. Ferrite

NPS were sonicated for 20 minutes to get a uniform size. Then we sprayed PLGA/acetone using a syringe pump (Multi-Phaser, NE-300, New Era Pump Systems, NY) keeping a flow rate at 0.3 ml/min and ultrasonic atomizer (Sonozap,2005) power, frequency at 3.5Watt, 130 kHz respectively. The droplets of PLGA were sprayed into 1% PVA (50ml) having 20 mg of ferrite NPs in it acting as an aqueous phase for encapsulation and left for magnetic stirring at 1500 rpm. Then after completion of spraying, the residual acetone was evaporated by heating at 50-55 °C for 10-15min on a magnetic stirrer under 600-800rpm. Then this formulation was centrifuged using ultracentrifuge (Optima XPN-80 Beckmann Coulter, Inc.) at 70,000-80,000g for a 25-30 min cycle and further washing was done with the distilled water three times in a row. Then after washing the pellet was lyophilized for further drying up overnight until it becomes dry completely. The dried NPs were then placed at 4 °C for future analysis and characterization.

2.2.4 Synthesis of Pip-PLGA-Magnetic (PFP) Nanohybrid

PFP nanohybrid system was synthesized by Ultrasonic atomizer with similar mentioned above method in which PLGA dissolved in Acetone sprayed in PVA worked as a surfactant which further stabilizes the droplets. 10 mg of Piperine (0.25% w/w) and 20mg of PLGA (0.5% w/w) was dissolved in acetone making the organic phase, and 1% PVA with 20mg ferrite nanoparticles made the aqueous phase. Ferrite NPS were sonicated for 20min to get a uniform size. Then we sprayed Pip-PLGA/acetone using a syringe pump (Multi-Phaser, NE-300, New Era Pump Systems, NY) keeping a flow rate at 0.3ml/min and ultrasonic atomizer (Sonozap,2005) power, frequency at 3.5Watt, 130 kHz respectively. The droplets of PLGA were sprayed into 1% PVA (50ml) having 20 mg of ferrite NPS in it acting as an aqueous phase for encapsulation and kept under magnetic stirring at 1000rpm. After completion of spraying, the residual acetone was evaporated by heating at

50-55 °C for 10-15 min on a magnetic stirrer under 600-800 rpm. Then this formulation was centrifuged using ultracentrifuge (Optima XPN-80 Beckmann Coulter, Inc.) at 70000-80000g for a 25-30 min cycle and further washing was done with the distilled water three times in a row. Then after washing the pellet was lyophilized for further drying up overnight until it becomes dry completely. The dried NPs were then placed at 4 °C for future analysis and characterization.

2.2.5 Encapsulation efficiency

The drug encapsulated inside nanoparticles per drug taken initially is termed as encapsulation efficiency and it is usually calculated by using two different approaches as follows:

1) Direct method- In this method, the amount of drug is directly calculated by taking reading using UV vis spectroscopy and then further comparing it with that of the calibration curve of piperine using the $y = mx + C$.

$$EE (\%) = A_1/A_0 \times 100$$

2) Indirect method- In this method, the reading of supernatant is usually subtracted from the concentration of the initial drug taken.

$$EE (\%) = [(A_0 - A_2)/A_0 \times 100]$$

A_1 = amount of drug loaded in the NPS; A_2 = amount of drug found in the supernatant; A_0 = amount of drug taken initially.

drug loaded in NPs per dry weight of the initial drug taken is known as encapsulation efficiency. It was calculated by using the Indirect method in which the reading was taken of supernatant and subtracted from the initial drug concentration to find out the encapsulation efficiency (Kaur et al., 2021).

The loading efficiency is drug loaded in the NPs per dry weight of nanoparticles formed.

2.2.6 *In vitro* drug release study

The *in vitro* drug release study was performed with the help of a dialysis membrane (10 – 14 kDa). Pip-encapsulated NPs were suspended again in PBS buffer (pH 7.4) having a concentration of 1mg/ml, in a dialysis bag and kept in a beaker having 60 ml PBS on a magnetic stirrer at 200rpm and a temperature of 37 °C. Then the periodic reading was taken for 7 days using a UV spectrophotometer. Every time 1ml of the solution was taken out for reading and the fresh PBS solution was added to maintain the entire volume. Then the comparison of the calibration curve which we plotted of piperine by making 10 different concentrations reading on a UV spectrophotometer was carried out to calculate the percentage release of the drug.

2.2.7 Study of *In vitro* cytotoxicity through MTT assay

The cytotoxicity of nanohybrids was calculated by performing MTT assay. Briefly breast cancer (MDAMB 231) cells were seeded in a 96 well plate in triplicate manner (8000 cells per well) and were left to grow in complete DMEM medium containing 10% FBS and 1% antibiotic. Cells were treated with nanohybrids for 48 h at 37° C, 5% CO₂. After incubation and adding 100 µl of MTT, (500 µg/ml in media) solution to each well, the plate was further incubated for 3 hours at 37°C to enable the intracellular reduction of the soluble yellow MTT to insoluble purple formazan crystals. The formazan crystals were dissolved by adding 100 µl of DMSO, and the absorbance was measured at 570 nm using a microplate reader. (Synergy™ H1 multi-mode microplate reader). Relative or percentage cell viability was calculated by normalizing the absorbance with respect to that of control.

2.2.8 Estimation of ROS production and nuclear organization

The HT29 and MDAMB 231 cells were seeded at similar densities and left overnight for adhesion. The nanohybrids were added at desired concentrations and incubated for 48 h. The cells were washed with DPBS. Then cells were stained with DCFDA (10 $\mu\text{g/ml}$) & incubated for 15 to 20 min at 37°C. The cells were also counterstained with Hoescht (5 $\mu\text{g/ml}$) for 10 min. Cells were visualized using confocal microscope (Olympus, model no. FV1200MPE, IX-83). The DCFDA was excited at 488nm and corresponding ROS was detected at 530nm. For Hoescht the excitation was 405 nm, and emission at 460 nm.

2.2.9 Dual staining of GF-AFC and propidium iodide (PI) for the assessment of live/dead cell population

The HT-29 cells were seeded at similar densities and left overnight for adhesion. The nanoparticles were added at desired concentration (50 $\mu\text{g/ml}$ and 100 $\mu\text{g/ml}$) and incubated for 72 hs. The protocol for the live/dead staining was performed by following the mentioned instructions. Briefly, the GF-AFC stock was added to the assay buffer at 1/1000 dilution and supplemented to the cells. The spent media which supposedly contain the floating dead cells were collected and stained with 10 $\mu\text{g/ml}$ PI. Both the cell populations were mixed and incubated for 20 min in dark. The fluorescent cells were visualized using a confocal microscope (Olympus, model no. FV1200MPE, IX-83), by exciting at 405 nm and 588 nm for GF-AFC and PI respectively.

2.2.10 Dual staining of Calcein AM and propidium iodide (PI) for the assessment of live/dead cell population

The MDAMB 231 cells were seeded at similar densities and left overnight for adhesion. The nanoparticles were added at desired concentration and incubated for 48 h. The protocol for the live/dead staining was performed by following the mentioned instructions. Briefly, the Calcein AM (1mg/ml) was added to the DPBS making final concentration of 1 μ g/ml and supplemented to the cells. The spent media which supposedly contain the floating dead cells were collected and stained with 10 μ g/ml PI. Both the cell populations were mixed and incubated for 20 min in dark. The fluorescent cells were visualized using a confocal microscope (Olympus, model no. FV1200MPE, IX-83), by exciting at 405 nm and 588 nm for calcein am and PI respectively.

Chapter 3

Results and Discussion of Applications of PFP

3.1 Preparation of UV-spectra of Piperine

The UV spectra works on the principle of Beer - Lambert law which states that the concentration and absorbance are directly proportional to each other. Using it we had a spectrum of Pip and CPT to check their specific absorbance peak and it was found to be significant.

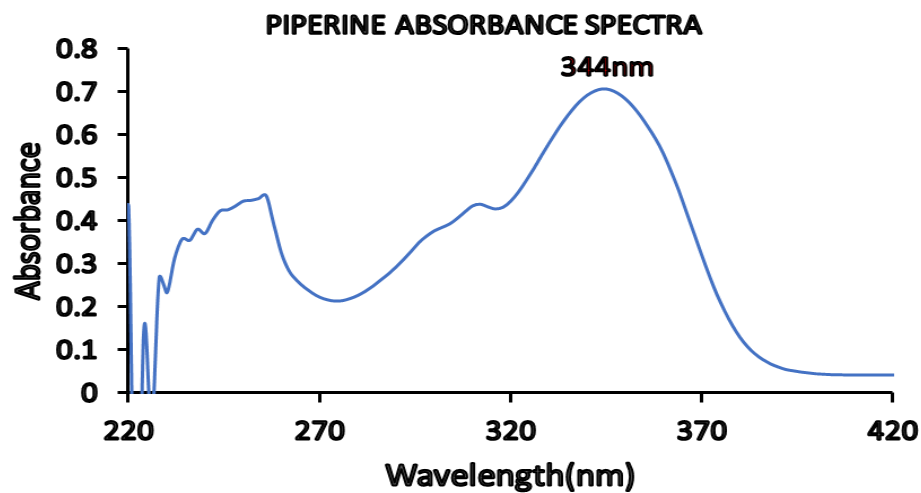


Figure 3. 1: UV spectra of piperine showing their specific peaks at 344 nm in DMSO

3.2 Preparation of calibration curves of Pip

Calibration curves were prepared using the principle of UV spectrophotometer by making 8-10 different concentrations in duplicate manner in DMSO and their absorbance were noted. Calibration curve provides the linearity coefficient and regression equation. These calibration curve shows that, the linearity co-efficient is near to 1 and

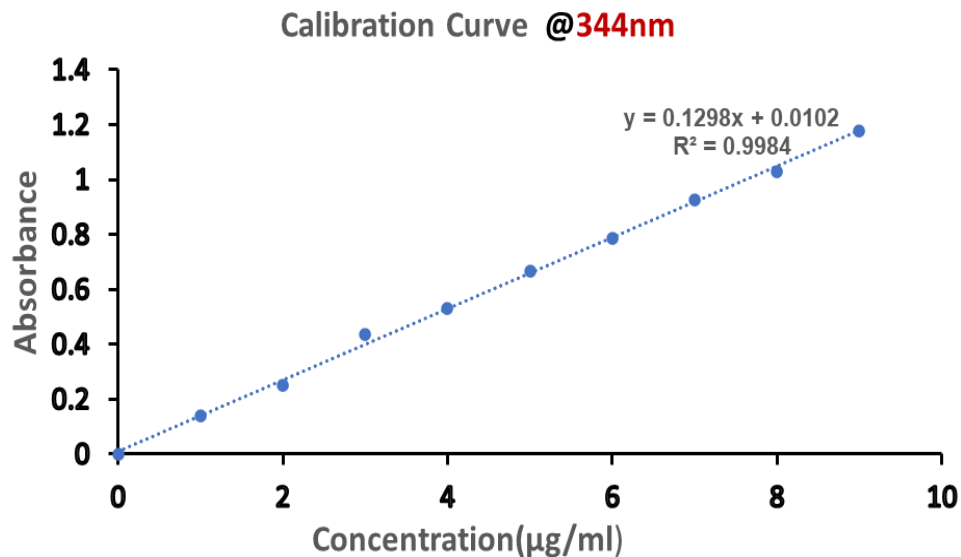


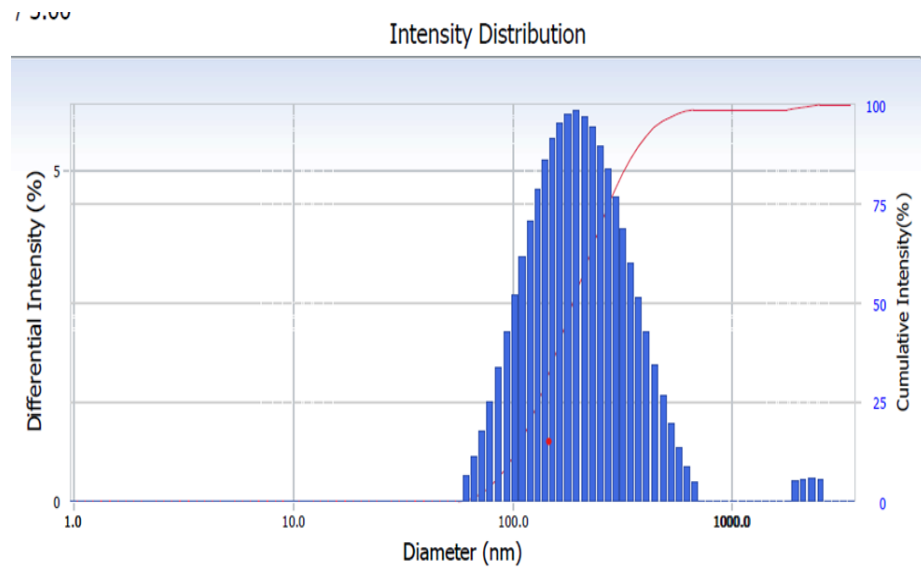
Figure 3. 2: Calibration curve of pip in DMSO prepared at 344nm

the drug obeys the Beer-lambert's law. The calibration curves were further used to calculate the encapsulation efficiency of drug encapsulated in nanohybrid system.

3.3 Characterization of MNP

3.3.1 Dynamic Light Scattering

The synthesized nanoparticles (NPs) exhibited desirable morphological traits, such as nano-size range, spherical shape, surface charge, and homogeneous dispersion, which facilitate effective biodistribution and pharmacokinetics studies. The particle size and polydispersity index were evaluated primarily through dynamic light scattering (DLS) using a Nano plus instrument, which is a widely adopted technique that enables the sizing of particles as small as 1 nm in diameter (Zürich, n.d.).



Cumulants Results

Diameter	(d)	: 251.7	(nm)
Polydispersity Index (P.I.) : 0.165			
Diffusion Const.	(D)	: 1.954e-008	(cm ² /sec)

Figure 3. 3: DLS analysis of magnetic NPs showcasing average size around 250nm with PI of 0.165 which tells about the uniformity of the NP in the solution form

DLS data showed the particle size distribution of average size of around 250nm that can be seen in the above figure 3.3 comprising polydispersity index of 0.165 showing uniformity in the sample.

3.3.2 Morphological analysis

The morphology (size, shape) study was done by FESEM. The morphology of magnetic NPs was found to be spherical and uniform in size that can be seen in the figure 3.4. MNPs have hydrophobic surfaces with larger surface area to volume ratio when present without any coating on its surface developing higher hydrophobic interactions due to which it agglomerates leading to increase in the particle size (Ali et al., 2016). The magnetic properties were confirmed by applying external magnetic field to the NP which showed considerable magnetization.

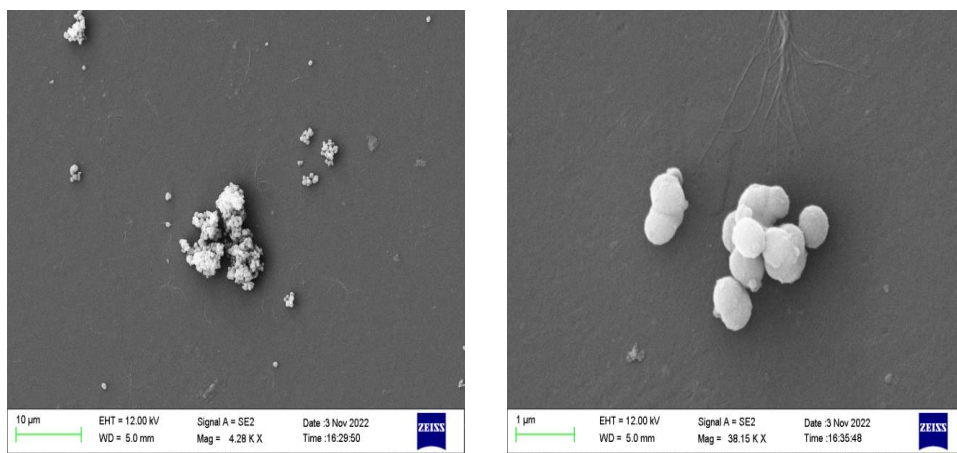


Figure 3.4: FESEM images of MNPs showing spherical entities.

b) The magnetization of MNPs when applied external magnetic field.

3.3.3 Confirmation of functional groups

To analyze the exact composition of magnetic NPs, we used FTIR spectrum (figure 3.5) which works on the IR light beam with various wavelengths is split into two equal parts using a beam splitter. (Butterfly, 2019). In this spectrum, Fe-O stretch appeared at around $600\text{-}700\text{ cm}^{-1}$, O-H stretch was observed at $3200\text{-}3600\text{ cm}^{-1}$, Fe-OH stretch at around $550\text{-}600\text{ cm}^{-1}$ respectively confirming the synthesis of magnetic NP as per various literature studies have noted the same (Sodipo and Abdul Aziz,

2014).

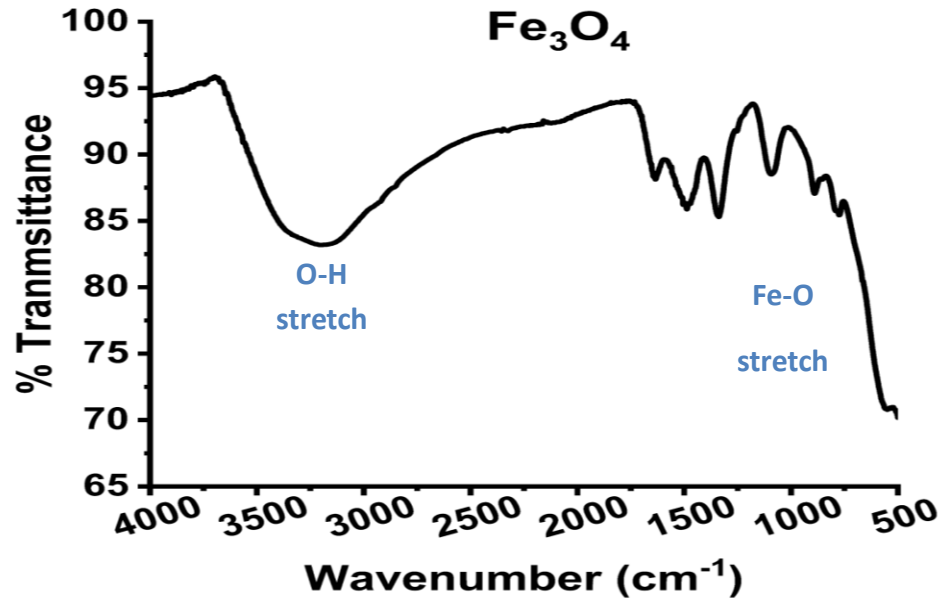


Figure 3.5: The FTIR spectra of magnetic NP having characteristic stretches.

3.3.4 Crystal characterization by XRD

The crystal structure of magnetic NP was confirmed with p-XRD. The XRD spectra of Fe_3O_4 nanoparticles typically show distinct diffraction peaks that correspond to the different crystal planes of the Fe_3O_4 lattice. The most prominent peaks are located at 2θ values of 30.1° (220), 35.5° (311), 43.3° (400), 53.5° (422), 57.1° (511), and 62.9° (440) (Bertolucci et al., 2015). There could be some shifts in the peaks of these NPs due to different orientation of magnetic domains in the crystal lattice. The peak broadening in the XRD spectra of Fe_3O_4 nanoparticles is typically due to the finite size of the nanoparticles.

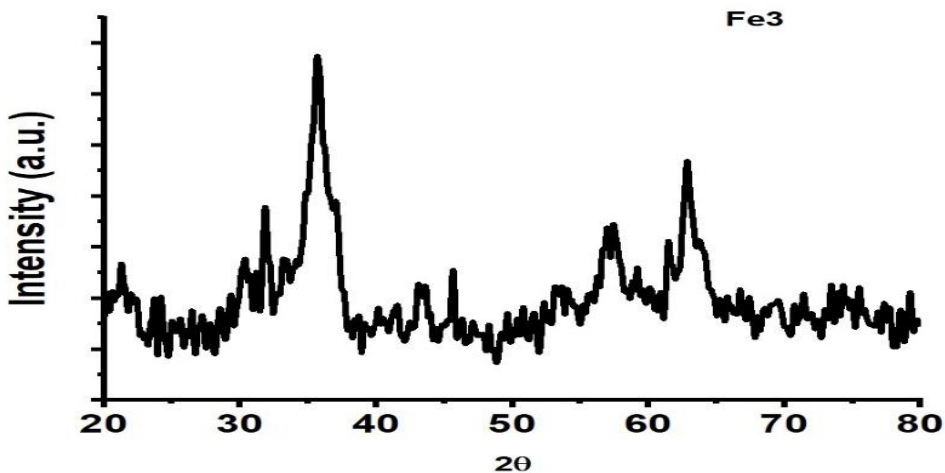
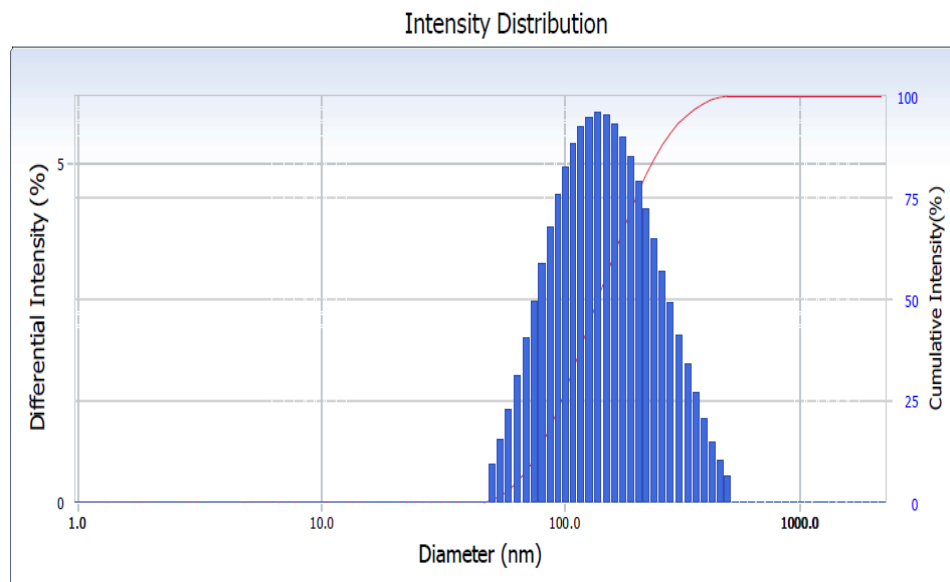


Figure 3.6: XRD spectra of magnetic NP showing characteristic peaks.

3.4 Characterization of PF:

The PF nano hybrids were used as vehicle control for the cellular studies. The synthesized NPs having morphological characteristics such as nano-size range, spherical shape, surface charge, homogeneous dispersion etc., helps conjointly in biodistribution and pharmacokinetics studies. Particles average size and dispersion (polydispersity index) was primarily characterized using DLS (Nano plus) as particle size analysis. The particles size was found to be quite uniform with the average size of 137nm that can be seen in the figure 3.7.



Cumulants Results

Diameter (d) : 137.6 (nm)
 Polydispersity Index (P.I.) : 0.181
 Diffusion Const. (D) : 3.574e-008 (cm²/sec)

Figure 3. 7: DLS analysis of PF nanohybrid showcasing average size around 137 nm with PI of 0.181 which tells about the uniformity of the NP in the solution form.

The morphological analysis was done through FESEM showing uniform shape and size of the nanohybrids which can be seen in the figure 3.8. EDX analysis was also performed simultaneously with SEM. During EDX measurement, different areas were analyzed to check the homogeneity and elemental distribution of synthesized structure. The presence of iron can be seen in the corresponding peaks confirming incorporation of iron in the PLGA nanoparticles. Details of the EDX spectra of the PF nanohybrids values show the weight percentage and atomic percentage (figure 3.9). As per morphological studies, it was found to be uniform and consistent, suitable to be used in further studies.

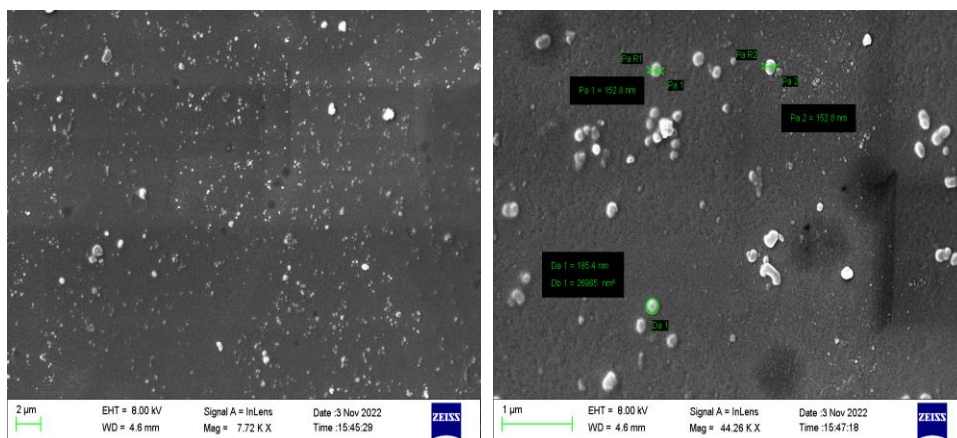


Figure 3. 8: SEM images of PF nanohybrid showing uniformity in size and shape.

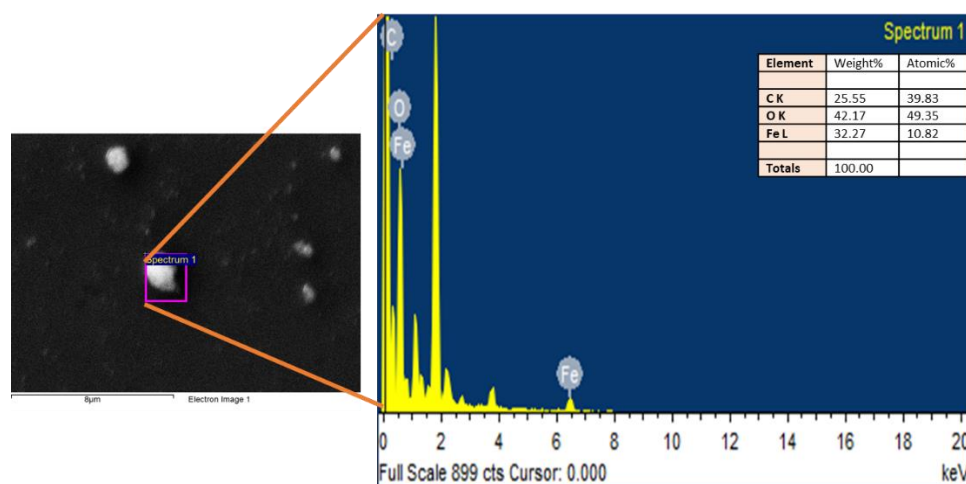


Figure 3. 9: EDX spectra of PF single nanohybrid confirming the incorporation of PLGA-iron oxide nanoparticles. The spike of Fe can be seen in the figure in between 0 and 2 of x-axis.

Further confirmation of PF incorporation was done through XRD spectroscopy showing the little amorphous nature of PLGA while representing the presence of crystal moiety inside the nanohybrids due to magnetic NP which can be seen in the figure 3.10. The larger peak in between 10- 30° showing the presence of PLGA previously reported (Khanal et al., 2016) while the later peaks are of magnetic NP that can be matched with that of plain magnetic NPs discussed above confirming the incorporation of MNP with that of PLGA NPs.

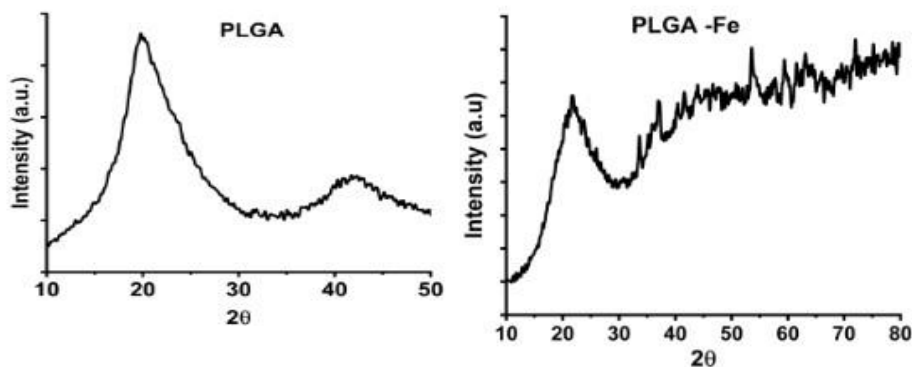
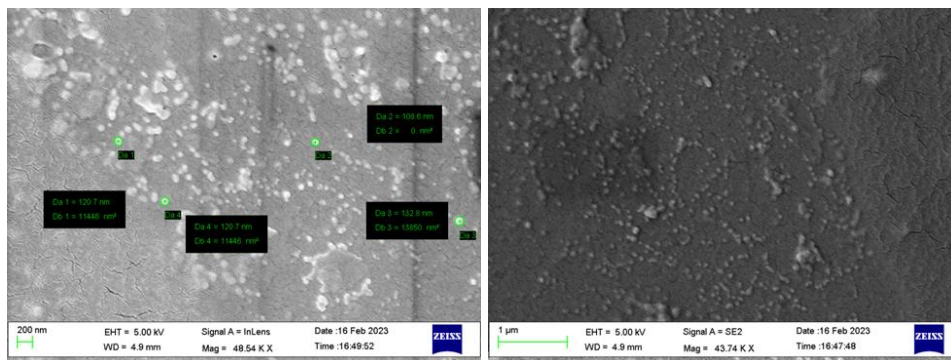


Figure 3. 10: The XRD spectra proving incorporation of PLGA and magnetic NPs.

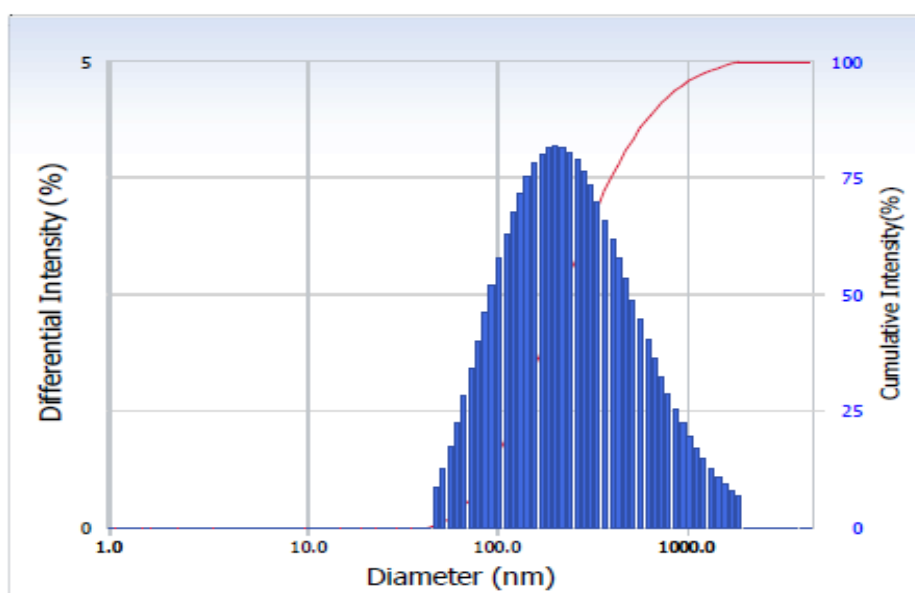
3.5 Characterization of PFP

The morphological analysis was done through FESEM showing uniform shape and size of the nanohybrids which can be seen in the figure (3.11 a). These were found to be suitable for the cellular uptake crossing the various kinds of barriers in our circulatory system. The size of these nanohybrids was found to be little larger when checked using DLS than that of SEM. The possible reason behind it could be the agglutination or aggregation of the nanohybrids in aqueous phase leading to showing larger average size.

The synthesized NPs having morphological characteristics such as nano-size range, spherical shape, surface charge, homogeneous dispersion etc., helps conjointly in biodistribution and pharmacokinetics studies. Particles average size and dispersion (polydispersity index) was primarily characterized using DLS (Nano plus) as particle size analysis. The particles size were found to be quite uniform with the average size of 247nm that can be seen in the figure 3.11b.



(A)



Cumulants Results

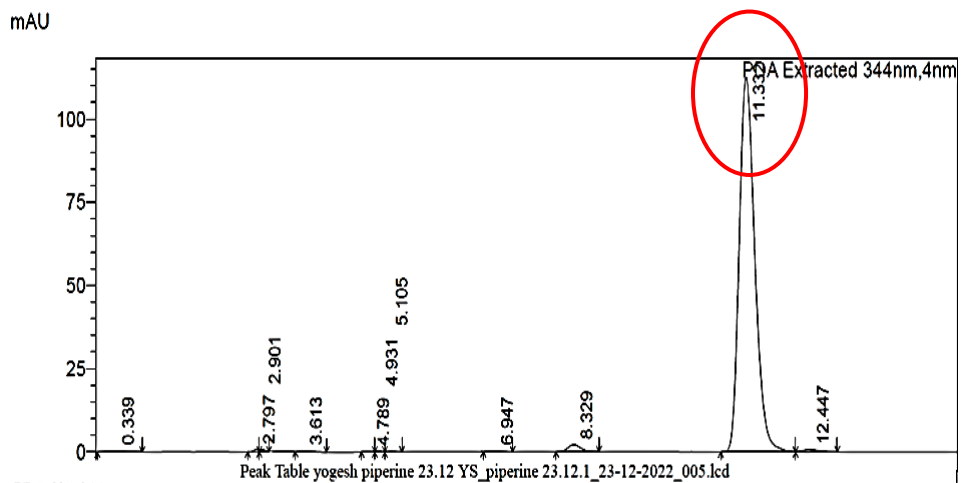
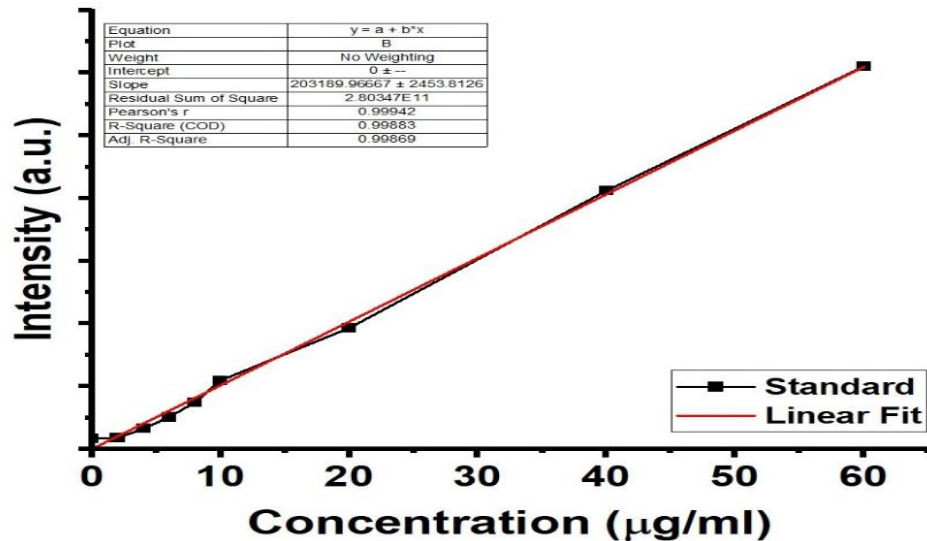
Diameter (d) : 247.1 (nm)
 Polydispersity Index (P.I.) : 0.214
 Diffusion Const. (D) : 1.991e-008 (cm²/sec)

(B)

Figure 3. 11: a) SEM images of PFP nanohybrid system. b) DLS analysis of nanohybrids.

3.6 Encapsulation efficiency determination

The encapsulation efficiency of synthesized PFP nanohybrids was calculated using indirect method which includes comparison of the supernatant reading with that of calibration curve of piperine prepared earlier during which we got the straight-line equation. The encapsulation efficiency of the same was also calculated using HPLC having retention time (RT) of around 11.5min. The standards were prepared in DMSO with multiple concentrations and then HPLC was performed to calculate the accurate amount of the drug encapsulated inside nanohybrid system. After evaluating the average encapsulation efficiency was found to be around $82 \pm 5\%$ in all the synthesis with the average loading efficiency of $25 \pm 5\%$.



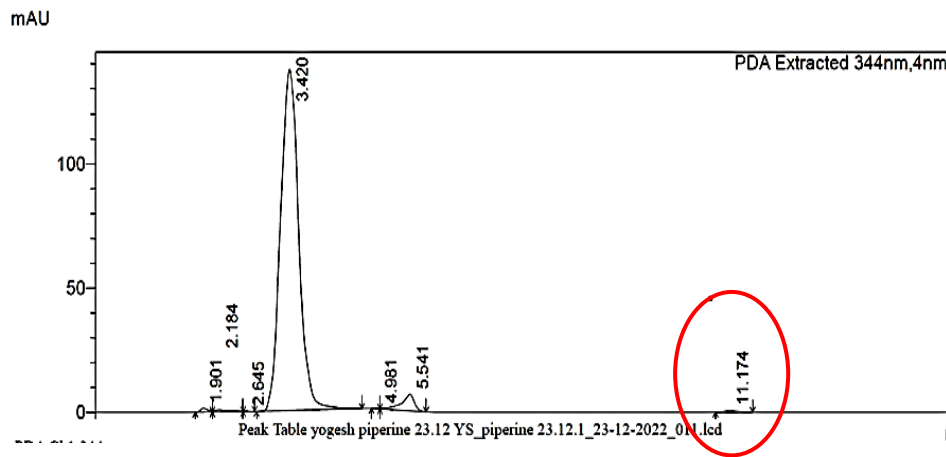
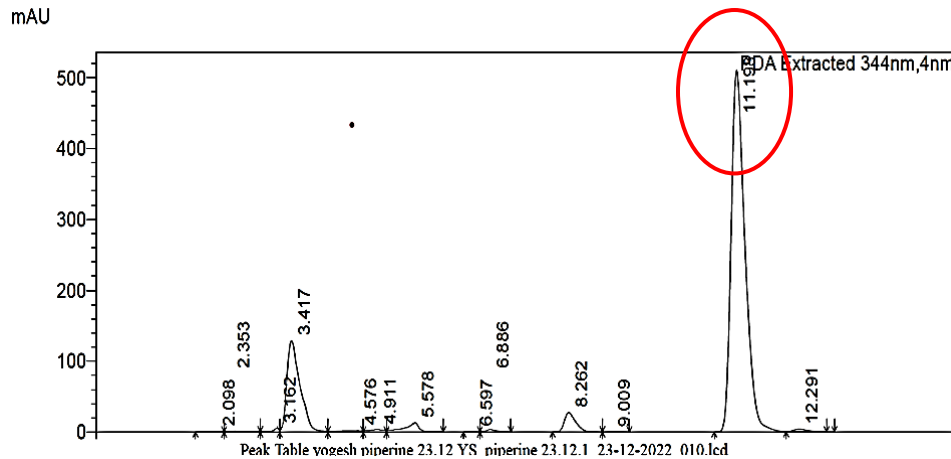


Figure 3. 12: a) calibration curve of pip/DMSO prepared by using HPLC

b) HPLC graph of one of the standard runs to compare the retention time of pip

c) HPLC graph of first and second supernatant after centrifuge washing showing the peak intensity at similar retention time (the various smaller peaks in the supernatant could be of PVA, unsettled PLGA, magnetic materials.)

3.7 *In vitro* Pip release study

The release study of drug was done using the dialysis bag at pH 7.2 in PBS buffer for 7 days. There was initial burst out of drug was found out in initial 12-15h and it was very sustained release of drug later on leading to almost equilibrium stage after 72 h. The initial burst out was of around 9% in 12 h and then around 12% after 72 h. Sudden burst shows an approximate amount of drug tagged on the surface of the nanohybrid system leading to the release of it in very less amount of time. Because there was very sustained and controlled release of drug even after 4 days makes it suitable drug delivery vehicle for various studies enhancing bioavailability and further stability.

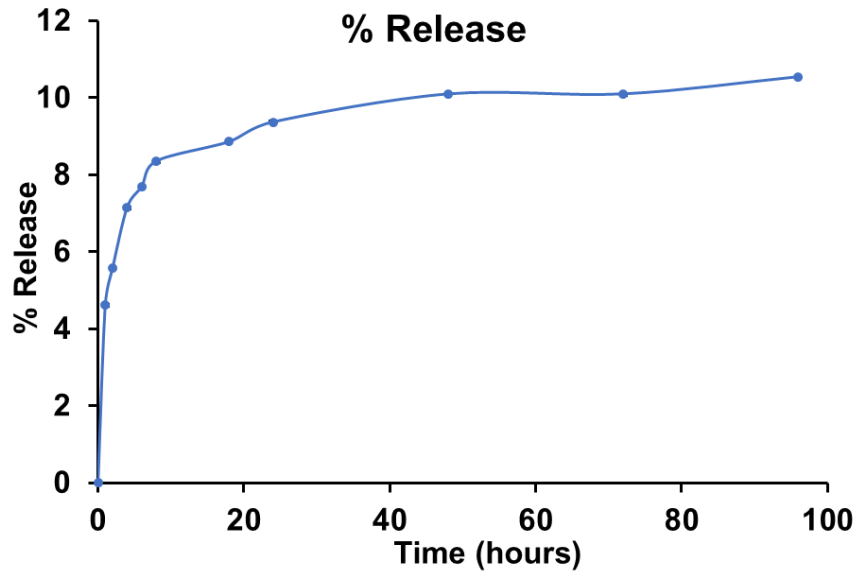
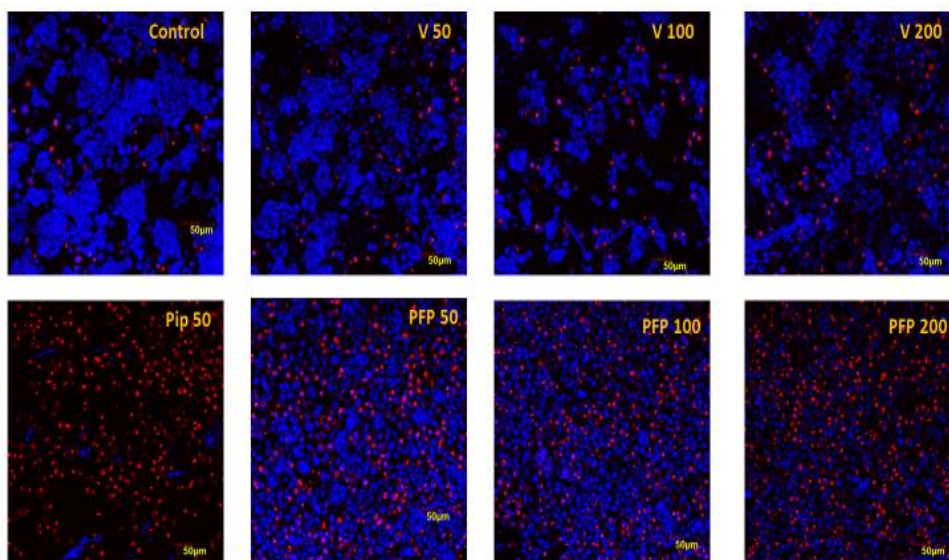


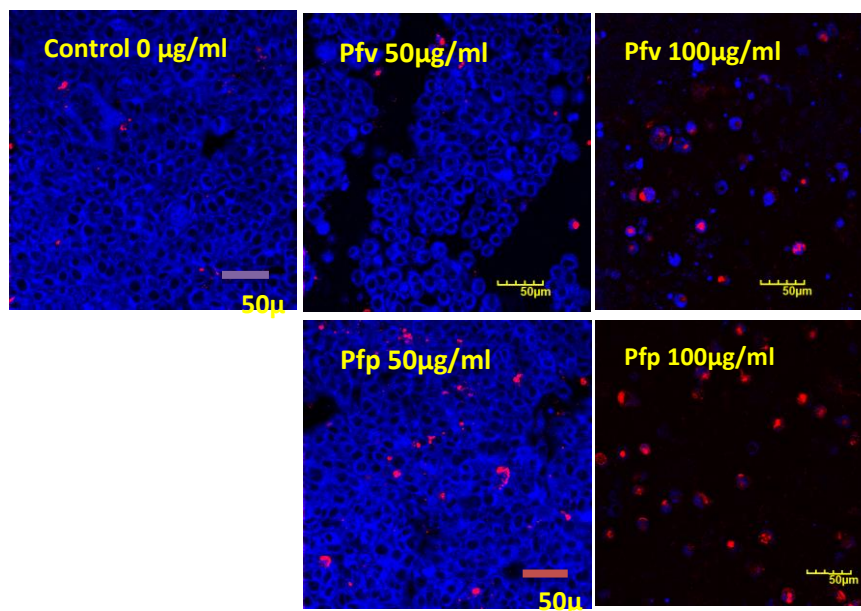
Figure 3. 13: *In vitro* drug release study from PFP nanohybrids

3.8 Live-dead cell imaging through GF-AFC and PI staining

Live and dead assay was performed to analyze the cytocompatibility and cytotoxicity of PF and PFP nanohybrids respectively on HT 29 cells using GF-AFC and PI staining dyes. This resulted in the cytocompatibility of vehicle (V/pfv) while drug loaded nanohybrids (PFP) were found to be toxic leading to the cellular deaths after 48 h and 72 h when analyzed using confocal microscopy that is visible in the figure 3.14. Blue color-stained cells are showing the live viable cells while red color-stained cells represent the dead cells. At higher concentration of drug loaded NP the red color-stained cells are higher in comparison to the control or lower concentration nanohybrid. In fact after 72 h even vehicle also showed considerable cellular deaths that can be seen in the respective figure 3.14 b.



(A)



(B)

Figure 3. 14: CLSM images of HT 29 cells stained *with GF AFC* and PI dyes showing live and dead cells in blue and red color respectively (A) for 48 h and. (B) for 72 h. V, pfv 50 ,100,200 and PFP 50, 100, 200 represents the concentration of PF and PFP in respective $\mu\text{g/ml}$. pip 50 represents concentration of pip in $50 \mu\text{g/ml}$ taken as positive control.

3.9 *In vitro* cytotoxicity assay

The cytotoxicity effect of free pip and nanohybrids was calculated by performing MTT assay. It was performed for a time of incubation of 48 h and 72 h having the dose concentration in $\mu\text{g/ml}$ for free and encapsulated inside nanohybrids as well. As a control all the concentrations of unloaded nanohybrids were taken to check their cytocompatibility with the HT-29 cancer cells (attached in appendix) while drug loaded nanohybrids were also treated to the cancer cells. The MTT of free drug showed comparable results with IC_{50} value around $19 \mu\text{g/ml}$ (Yaffe et al., 2015). The MTT of PFP at 48 h showed some discrepancies which is attached with appendix. The MTT studies showed around 80% of cell viability with unloaded NP while the cell viability considerably decreased with that of drug loaded nanohybrids. At 100

$\mu\text{g/ml}$ concentration of PFP, the cells viability was about 50% that can be seen in figure 3.15(C).

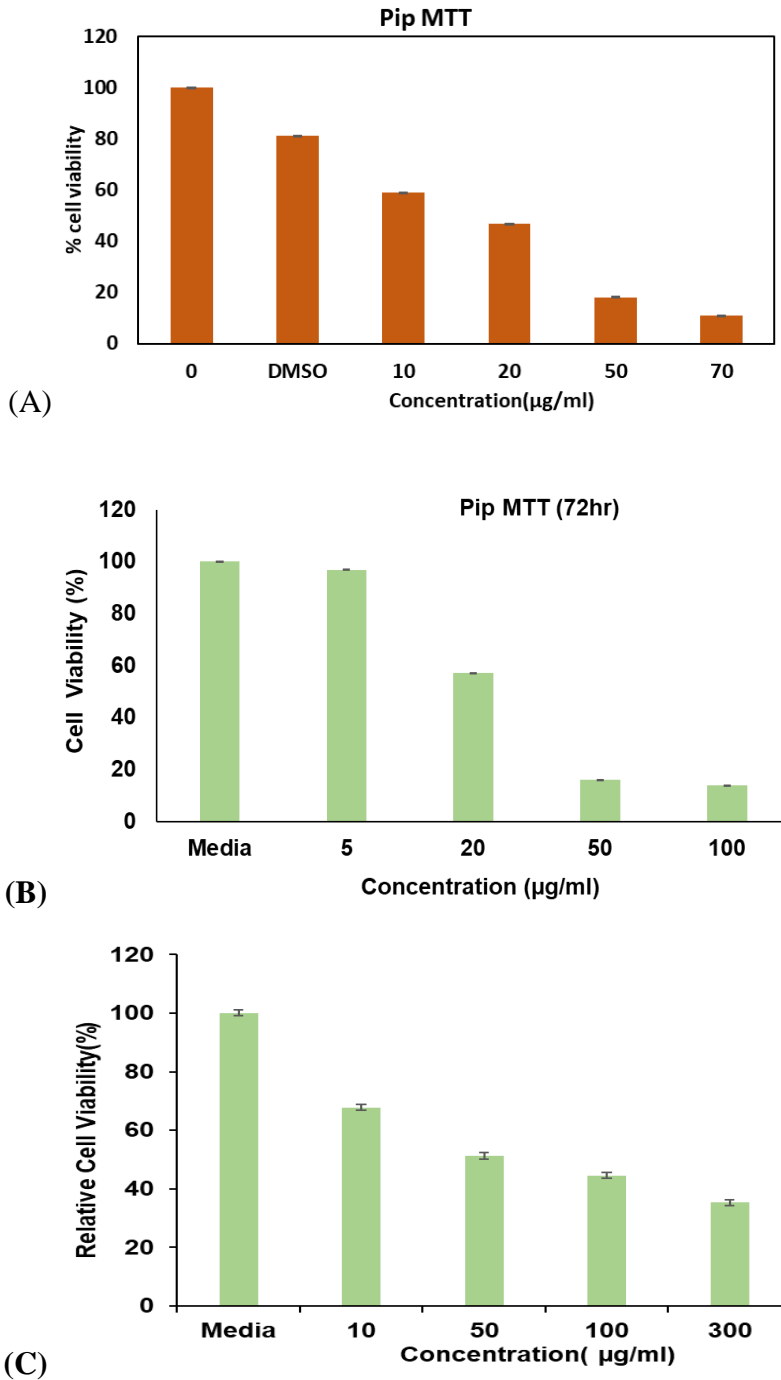


Figure 3. 15: MTT results of (A) and (B) free pip on HT cells after 48 h and 72 h respectively. (C) MTT of treatment of PFP on HT 29 cells after 72 h.

3.10 ROS production

The excessive ROS production leads to oxidation of major biomolecules causing cell damage in various cancer cell lines. Piperine also leads to production of ROS inside the cells in an increasing way as per the concentration of the drug treated increases (Siddiqui et al., 2017). This ROS production is detected with the increasing intensity of DCFDA fluorescence due to oxidation of it by oxygen free radicals. PFP nano hybrids also showed considerable increase in ROS production as per the treatment of drug loaded nano hybrids increased in comparison to that of control. This further leads to the initiation of early apoptosis activated by ROS production. The increased ROS production can easily be seen in the figure 3.16 and 3.17 as the concentration of drug loaded nano hybrids increased the green colour intensity further increased respectively when treated to MDAMB 231 and HT 29 cells respectively.

3.10.1 Nuclear organization study

Pip also leads to fragmentation of nuclear bodies inside the cells which further leads to apoptosis (Siddiqui et al., 2017). As per the CLSM images (figure 3.16) it was clearly visible that as the concentration of drug loaded nano hybrids increase, the integrity of the nucleus inside is declining consistently when treated with drug loaded nano hybrids on MDAMB 231 cells. The gradual release of drug from the nano hybrids showed considerable effect on nuclear organization as well.

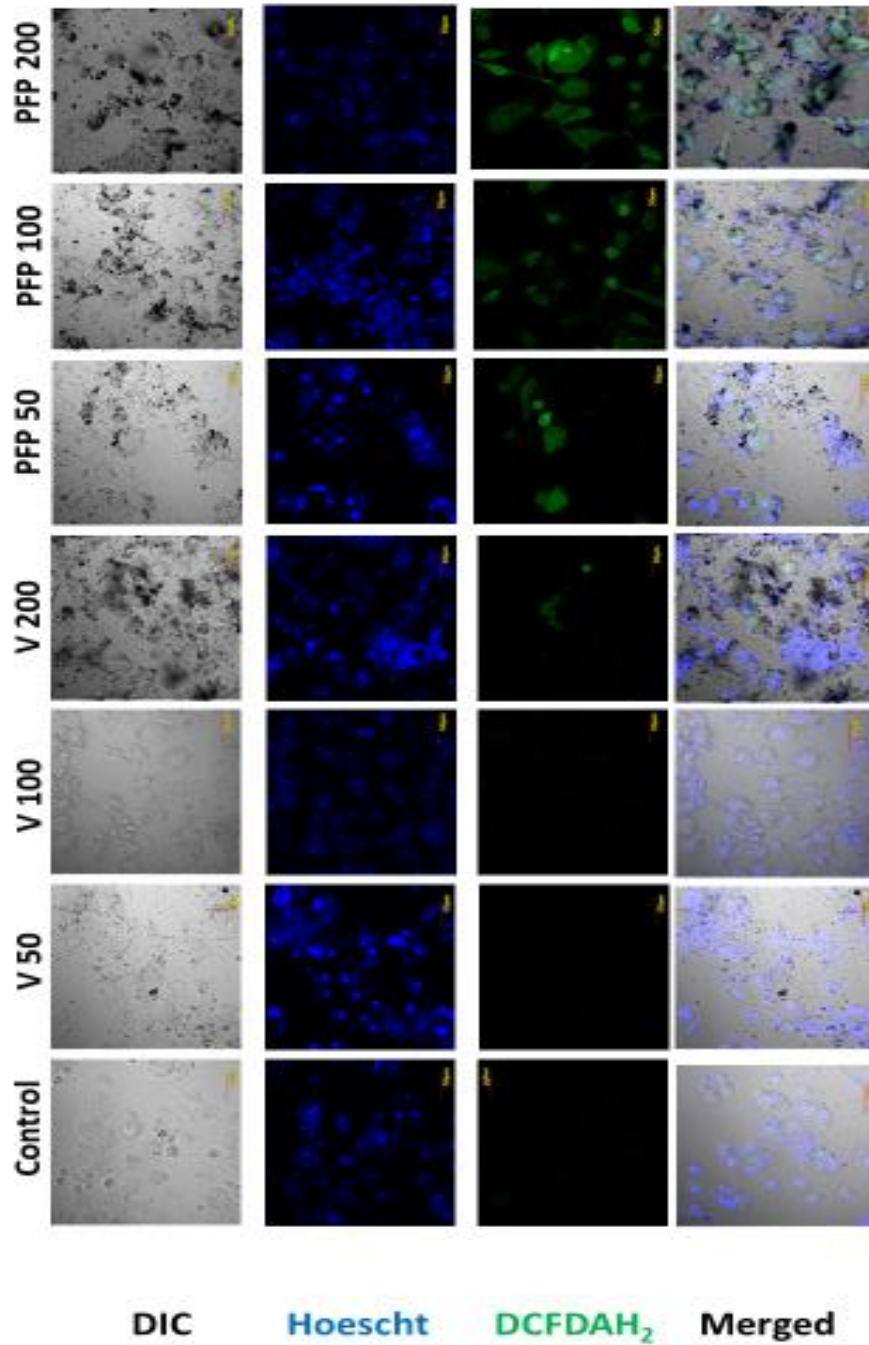


Figure 3. 16:- CLSM images of MDAMB 231 showing ROS & nuclear organization in green & blue color respectively. V 50, 100, 200 and PFP 50, 100, 200 represents the concentration of PF and PFP in respective $\mu\text{g/ml}$.

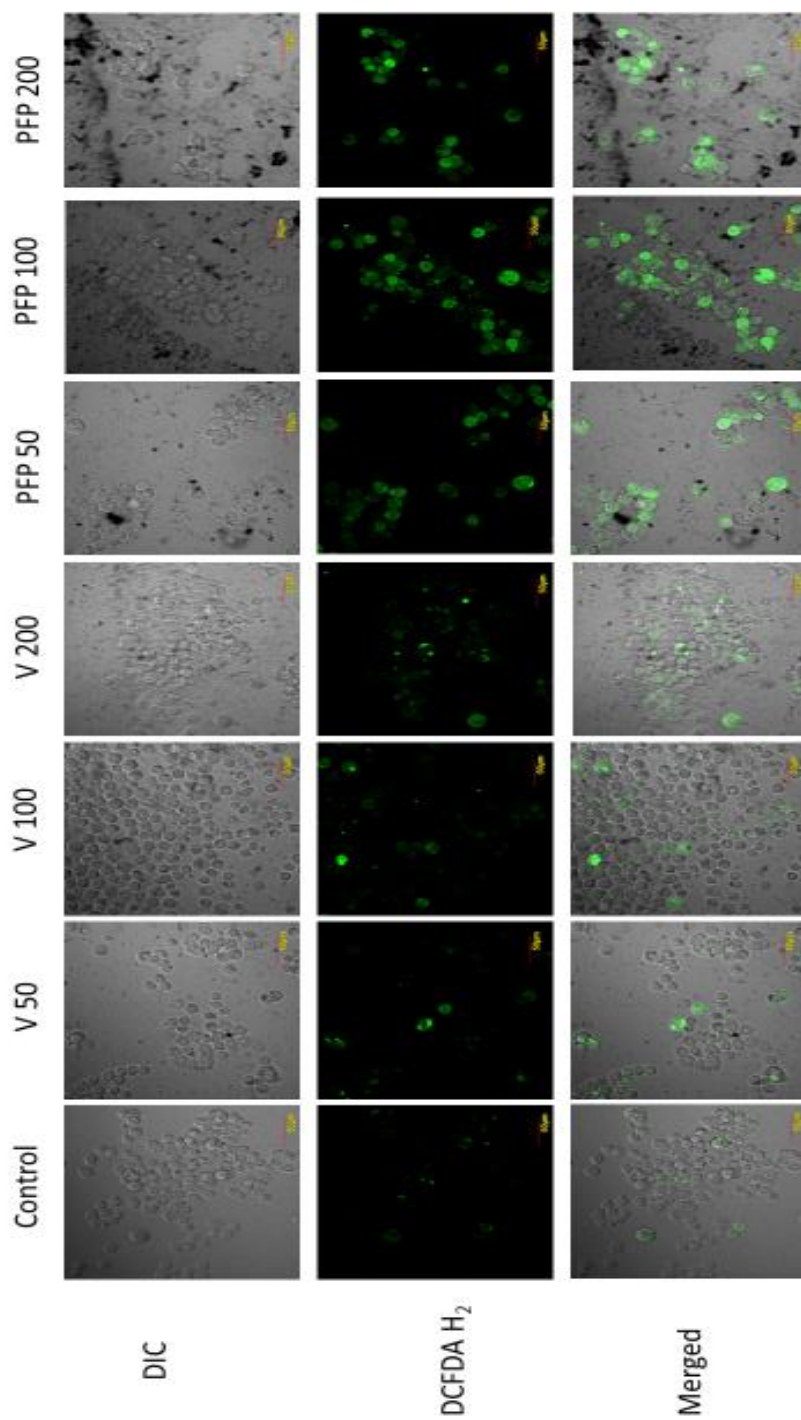


Figure 3. 17: CLSM images of HT 29 cells showing ROS in green color. V 50, 100, 200 and PFP 50, 100, 200 represents the concentration of PF and PFP in respective $\mu\text{g/ml}$.

3.11 Live and dead imaging

Live and dead assay was performed to analyze the cytocompatibility and cytotoxicity of PF and PFP nanohybrids respectively on MDAMB 231 cells using Calcein am and PI staining dyes. This resulted in the cytocompatibility of vehicle (PF) while drug loaded nanohybrids were found to be toxic leading to the cellular deaths after 48 hours when analyzed using confocal microscopy that is visible in the figure 3.16. Green color-stained cells are showing the live viable cells while red color-stained cells represent the dead cells proportions. As the concentration of drug loaded NP increased the increasing PI-stained cells was observed showing the cytotoxicity of pip. Pip was taken as positive control.

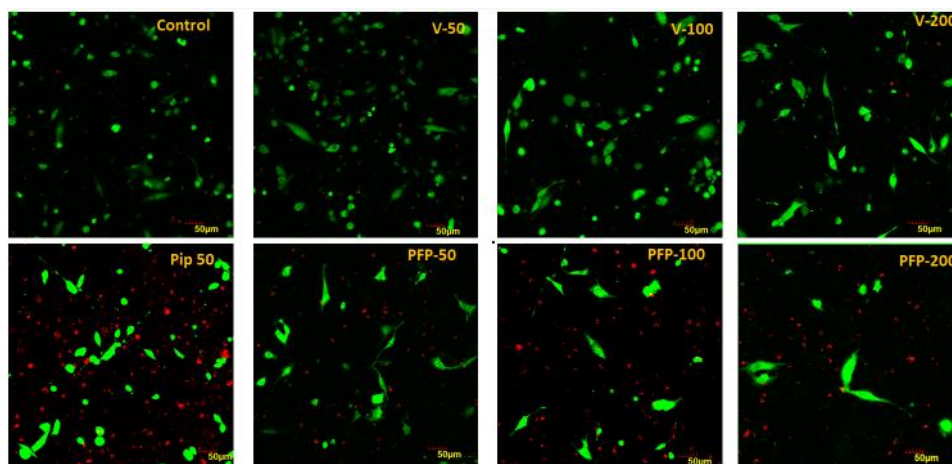


Figure 3. 18: CLSM images of MDAMB 231 cells stained with calcein am and PI dyes showing live and dead cells in green and red color respectively. V 50 ,100,200 and PFP 50, 100, 200 represents the concentration of PF and PFP in respective $\mu\text{g/ml}$. pip 50 represents concentration of pip in 50 $\mu\text{g/ml}$ taken as positive control.

3.12 Conclusion and future aspects

PLGA-magnetic-piperine nanohybrids have emerged as a promising drug delivery system for cancer therapy. The combination of biodegradable and biocompatible PLGA polymer, magnetic nanoparticles, and piperine offers several advantages over traditional chemotherapy, including sustained drug release, enhanced targeting and responsivity minimizes, agglomeration with good yield, leading to combinational theranostic approach with enhanced therapeutic efficacy. The incorporation of magnetic nanoparticles enables site-specific delivery of drugs to cancer cells on applying magnetic field and bioimaging, while the sustained release of the drug from the PLGA matrix ensures a prolonged therapeutic effect. This dual property comprising PF nanohybrid system was synthesized by ultrasonic atomizer using double emulsification and solvent evaporation method which was further characterized by using various techniques. DLS showed uniformity and consistency in its size (240 nm), FESEM showed uniformity in overall spherical morphology, XRD confirmed the incorporation of both of these NPs comprising its characteristics peaks. The drug encapsulation and loading was quite good with around 80% of encapsulation and 25% of loading efficiency. Sustained drug release profile was observed with around 12% in first 72 h and gradual and slow release of it later on. The unloaded nanohybrids also showed considerable cytocompatibility till a certain concentration of 300 μ g/ml and 500 μ g/ml respectively when tested on different cancer cell lines (HT 29 and MDAMB 231) using MTT assay. The drug (pip) loaded nanohybrids showed considerable cytotoxicity towards cancer cells when tested in different time intervals. CLSM studies confirmed the ROS production and nuclear disintegration in a dose dependent manner when tested by staining the cells with their respective dyes. The unloaded nanohybrids also showed some significant ROS production in a dose dependent manner. Some cytotoxicity assays on HT 29 and MDAMB cells are still undergoing to check the overall efficacy of these nanohybrids.

In conclusion, PLGA-magnetic-piperine nanohybrids hold great potential as a novel and effective drug delivery system for cancer therapy. And further research in this area can lead to the development of more potent drug carriers which would be holding good efficacy and potential to improve the overall cancer treatment strategies.

Chapter 4

Characterization and Application of PFC nanohybrids

4.1 Characterization of CPT:

The UV spectra was noted by using UV spectrophotometer and the standard peak was obtained at 366nm wavelength by dissolving it in DMSO figure(4.1a). This peak was further used to prepare a standard curve figure (4.1b) of multiple different concentrations to get a linear straight-line equation which would be further used to evaluate the encapsulation efficiency of nanohybrid system.

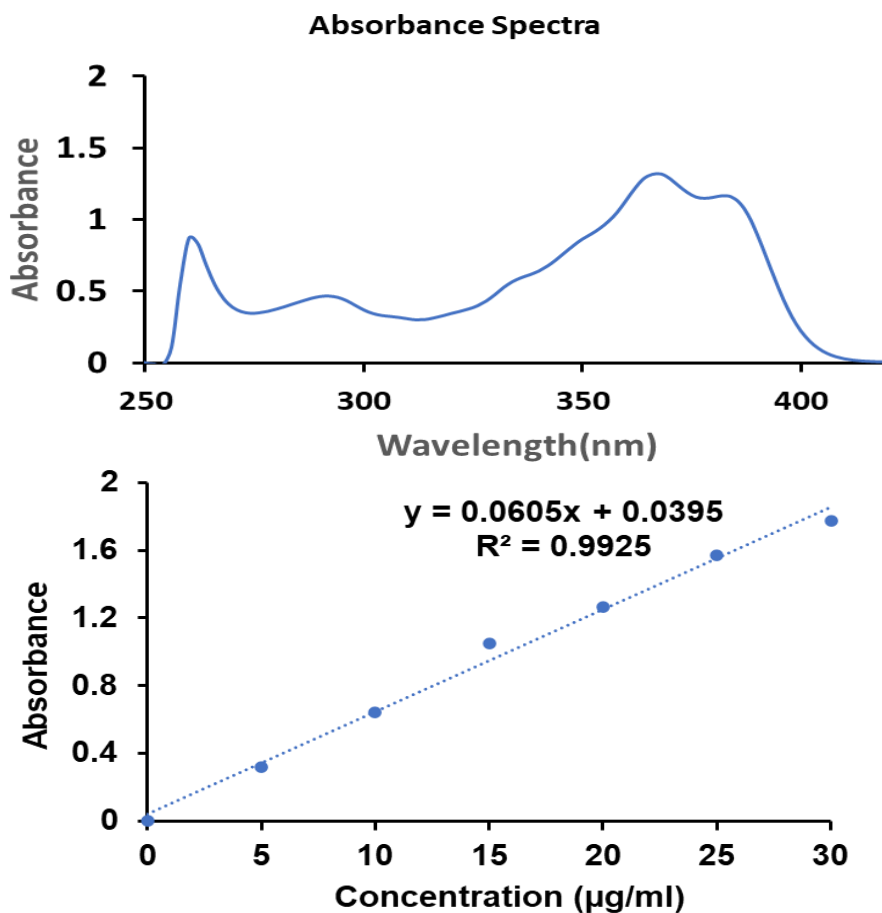


Figure 4. 1: (a) UV spectra of CPT/DMSO (b) calibration curve

4.2 Characterization of PFC nanohybrids:

The synthesized NPs having morphological characteristics such as nano-size range, spherical shape, surface charge, homogeneous dispersion etc., helps conjointly in biodistribution and pharmacokinetics studies. Particles average size and dispersion (polydispersity index) was primarily characterized using DLS (Nano plus) as particle size analysis. The particles size were found to be quite uniform with the average size of 300nm that can be seen in the figure 4.2.

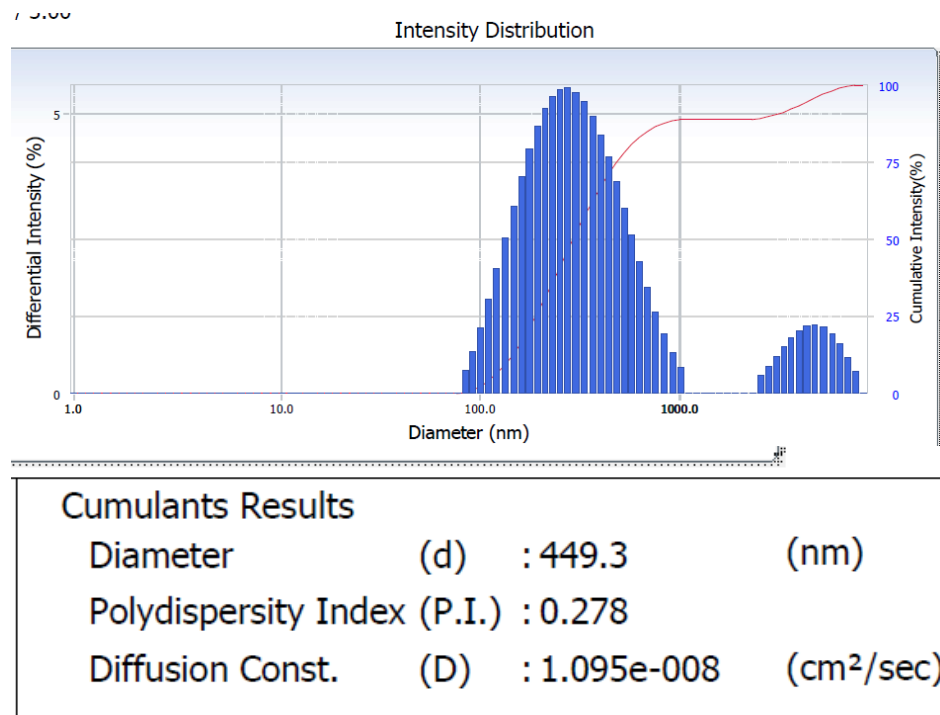


Figure 4. 2 : (a) : DLS analysis of PFC nanohybrids with PDI of 0.278.

The morphological analysis was done though FESEM showing uniform shape and size of the nanohybrids which can be seen in the figure 4.2 (b). These were found to suitable for the cellular uptake crossing the various kinds of barriers in our circulatory system. The size of these nanohybrids was found to be larger when checked using DLS than that of SEM.

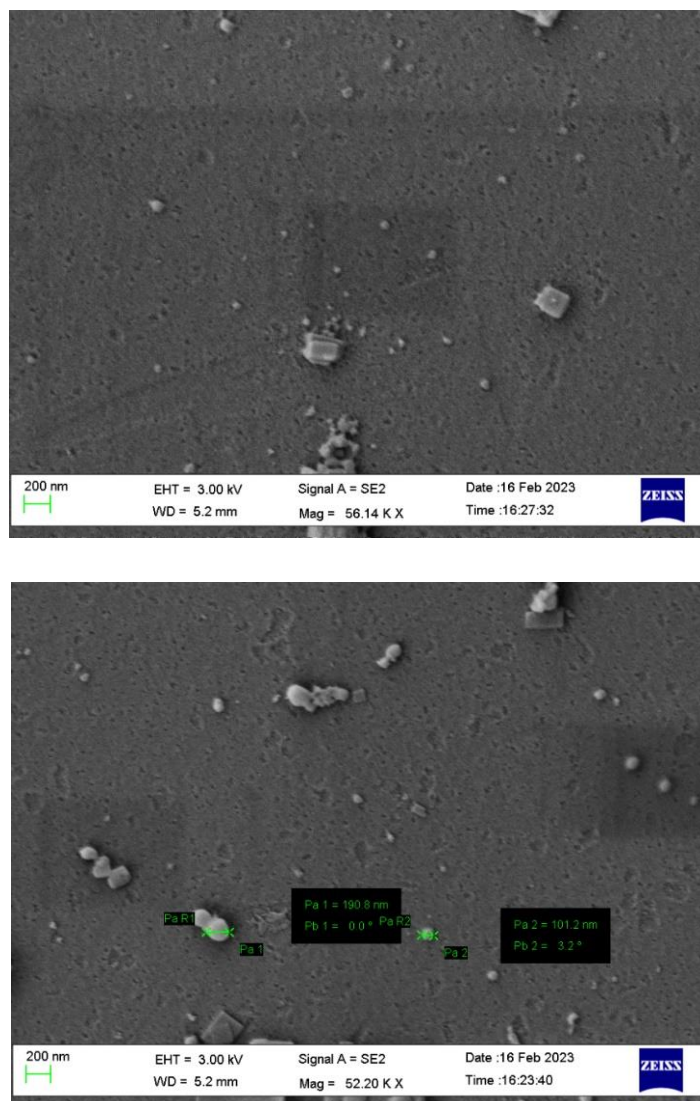


Figure 4. 3: (b): FESEM images of PFC nano hybrids

4.3 Encapsulation efficiency calculation:

The encapsulation efficiency of synthesized PFC nano hybrids was calculated using indirect method which includes comparison of the supernatant reading with that of calibration curve of CPT prepared earlier during which we got the straight-line equation. It was found out to be $94 \pm 5\%$ in repeated synthesis processes. Loading efficiency was found out to be $40 \pm 10\%$ in multiple synthesis.

4.4 *In vitro* drug release

The release study of drug was done using the dialysis bag at pH 7.2 in PBS buffer for 12 days. There was initial burst out of drug was found out in initial 12-15 h and it was very sustained release of drug later on leading to almost equilibrium stage after 72 h. The initial burst out was of around 9% in 12 h and then around 17% after 72 h. Sudden burst shows an approximate amount of drug tagged on the surface of the nanohybrid system leading to the release of it in very less amount of time. Because there was very sustained and controlled release of drug even after several days makes it suitable drug delivery vehicle for various studies enhancing bioavailability and further stability.

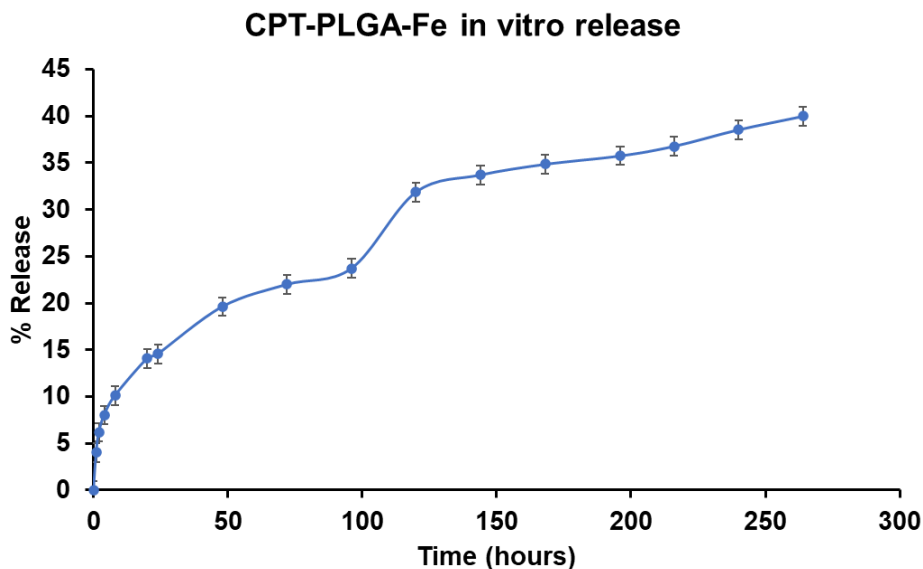


Figure 4. 4: in vitro drug release of CPT out of PFC nanohybrids

4.5 Conclusion and future aspects

CPT have shown tremendous results when applied to cancer cell but due to poor solubility and pharmacokinetics, it failed in enormous trials. To compensate this problem, we tried to synthesize nanohybrids of CPT loaded PLGA-magnetic nanohybrid system to enhance the overall efficacy and pharmacokinetics of this drug and also to explore the PLGA-magnetic nanohybrid potential to deliver this drug with quite accuracy. The PFC nanohybrids were synthesized using ultrasonic atomizer with . The PFC nanohybrid is still under optimization for further experiments. When characterized by using different techniques, these nanohybrid showed larger size of around 450nm in DLS and around 200 nm in FESEM. The encapsulation efficiency was found quite higher around 95% when calculated using UV-vis spectroscopy. The *in vitro* drug release profile showed sustained and gradual release form the nanohybrids when studied for 10-12 days with release percentage of around 40%. The cytotoxicity studies are still remaining as due to quite larger size of this nanohybrid system there is requirement of some further optimizations which will lead to smaller size comparatively increasing its theranostic potential as a suitable drug carrier against various carcinomas.

APPENDIX

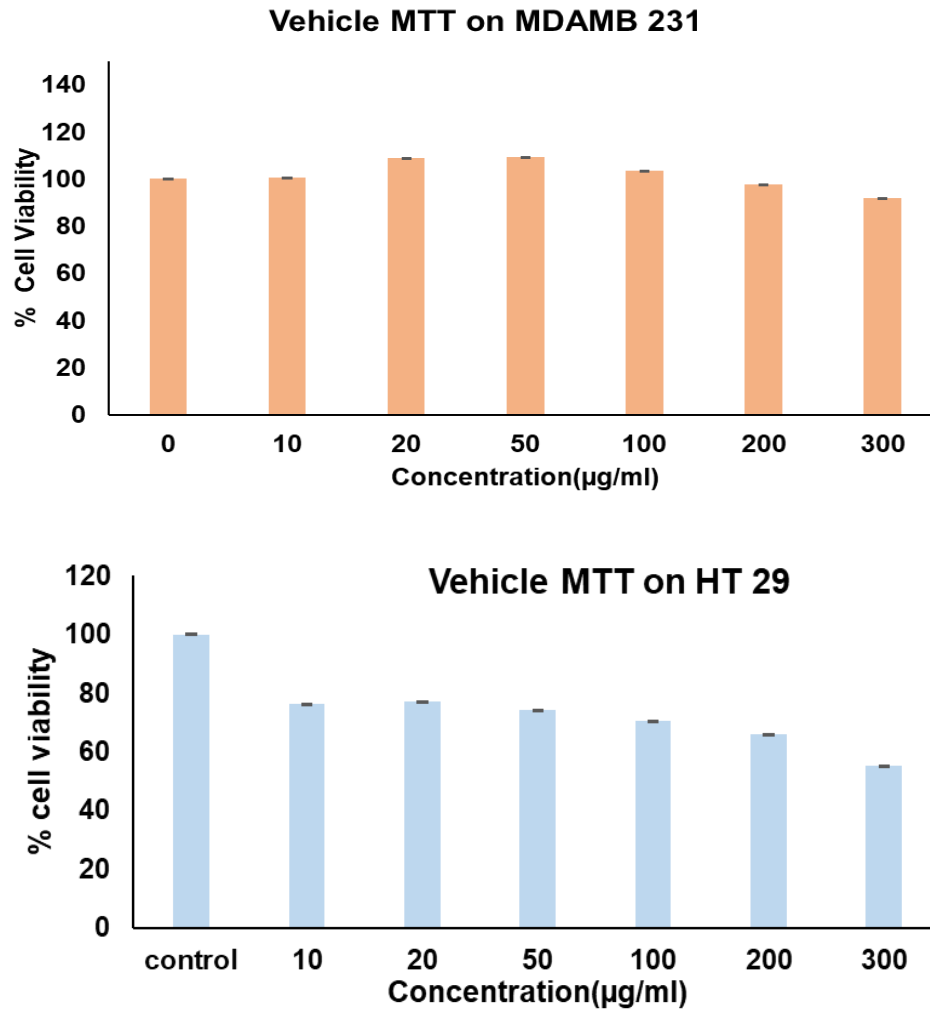


Figure A1 : MTT assay of PF on MDAMB 231 and HT 29 cells showing cytocompatibility of the PF nanohybrid at quite lower concentrations after 48 h.

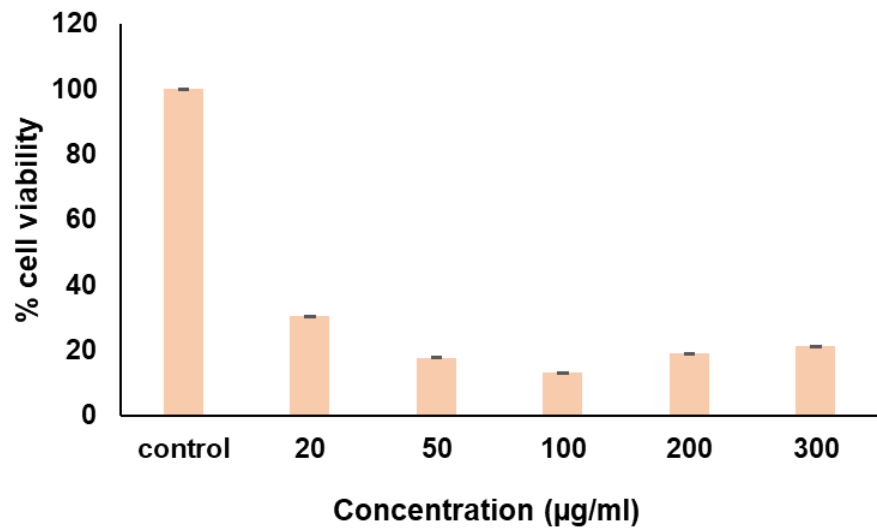
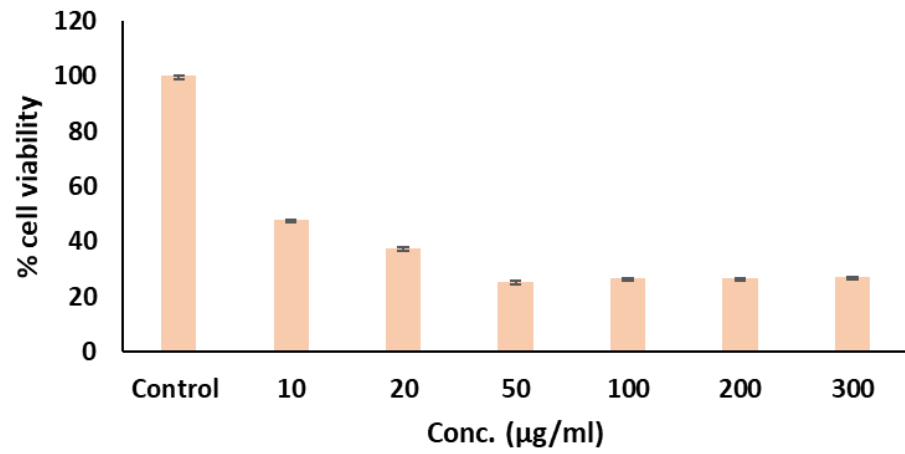


Figure A2: : MTT assay of PFP nanohybrids for 48 h on HT 29 cells

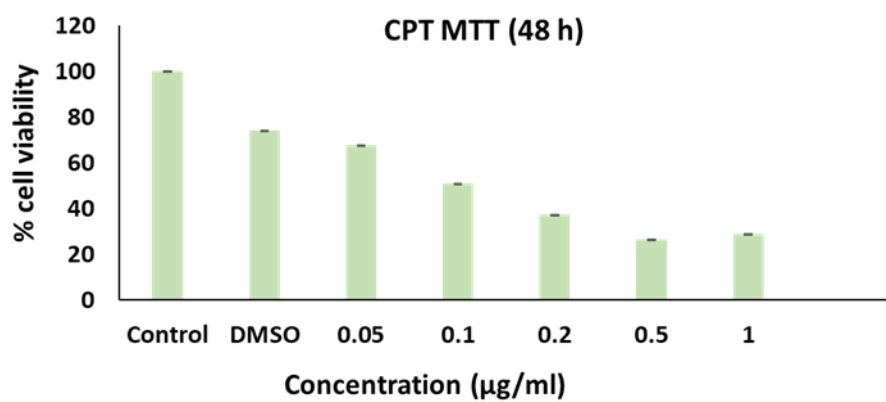
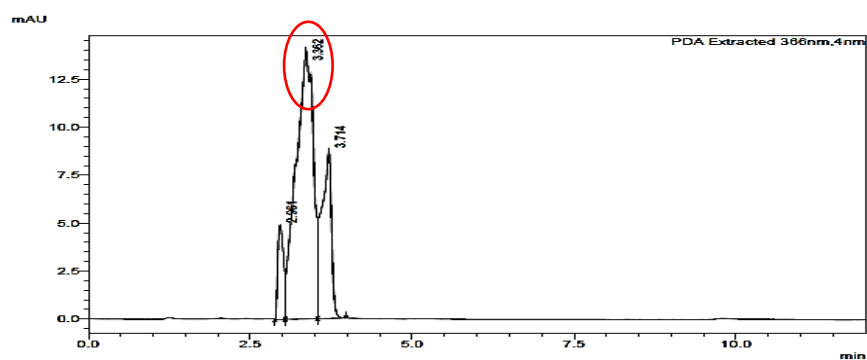
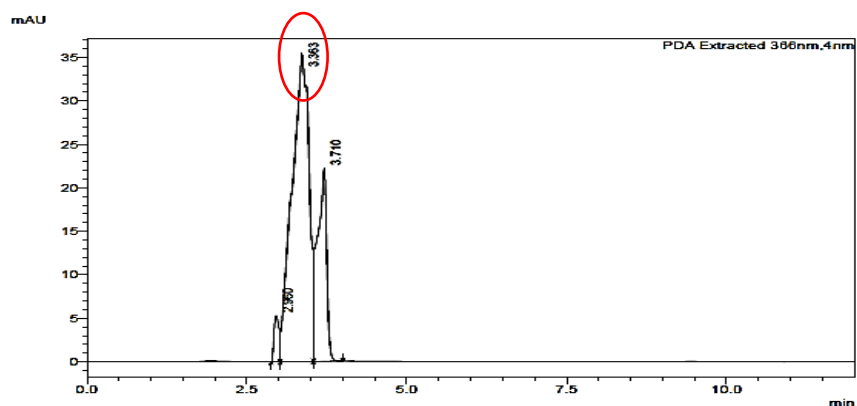


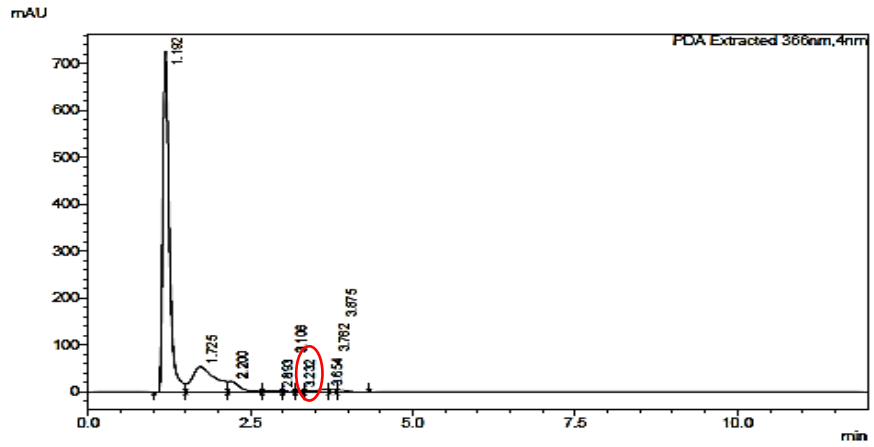
Figure A3: MTT assay of HT 29 cells after 48 h when treated with free CPT



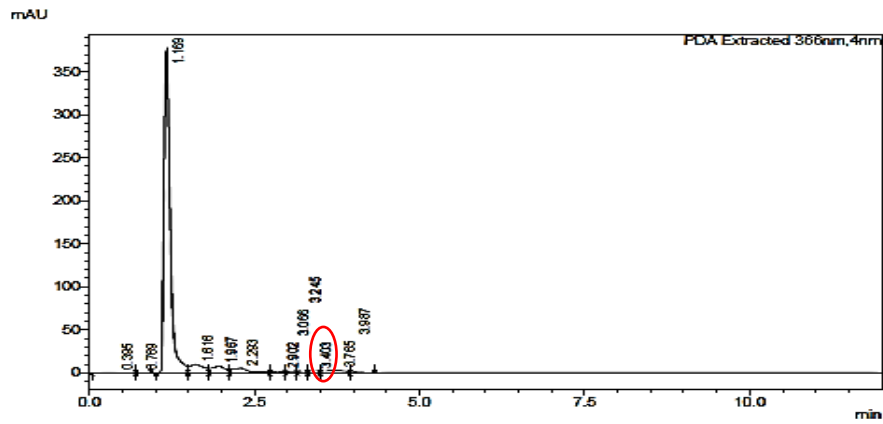
(A)



(B)



(C)



(D)

Figure A4: HPLC graphs of CPT to calculate encapsulation efficiency of PFC nano hybrid (standards and supernatants) having RT at 3.36 min.

(A) 5 μ g/ml (B) 12 μ g/ml (C) Supernatant 1 (D) Supernatant 2 after washing during centrifugation process.

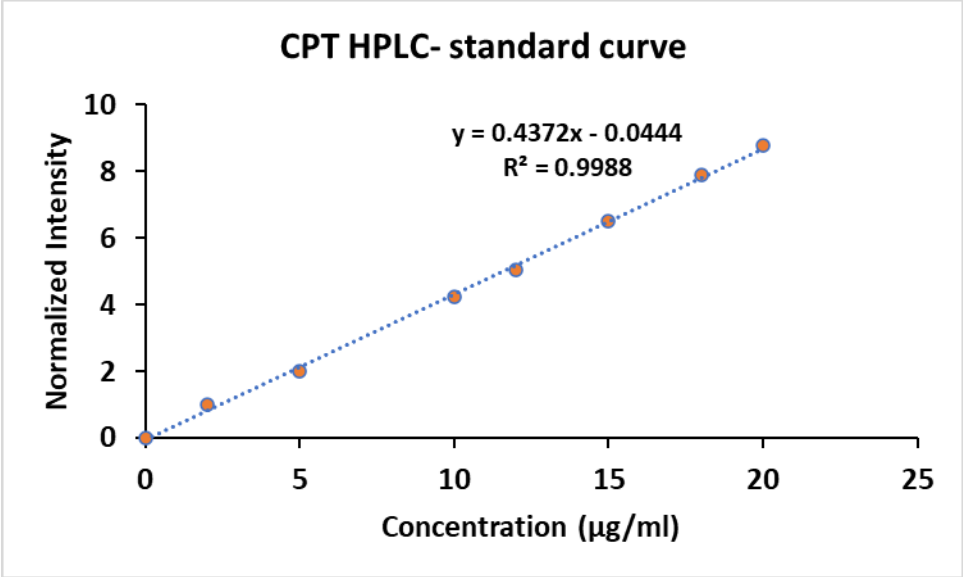


Figure A5: Calibration curve of CPT/DMSO prepared by using HPLC

REFERENCES

1. Ali, A., Zafar, H., Zia, M., ul Haq, I., Phull, A.R., Ali, J.S., Hussain, A., 2016. Synthesis, characterization, applications, and challenges of iron oxide nanoparticles. *Nanotechnol. Sci. Appl.* 9, 49–67. <https://doi.org/10.2147/NSA.S99986>
2. Almeida, A., Castro, F., Resende, C., Lúcio, M., Schwartz, S., Sarmiento, B., 2022. Oral delivery of camptothecin-loaded multifunctional chitosan-based micelles is effective in reduce colorectal cancer. *J. Controlled Release* 349, 731–743. <https://doi.org/10.1016/j.jconrel.2022.07.029>
3. Banerjee, S., Katiyar, P., Kumar, V., Saini, S.S., Varshney, R., Krishnan, V., Sircar, D., Roy, P., 2021. Black pepper and piperine induce anticancer effects on leukemia cell line. *Toxicol. Res.* 10, 169–182. <https://doi.org/10.1093/toxres/tfab001>
4. Bao, H., Zhang, Q., Yan, Z., 2019. The impact of camptothecin-encapsulated poly(lactic-co-glycolic acid) nanoparticles on the activity of cytochrome P450 in vitro. *Int. J. Nanomedicine* Volume 14, 383–391. <https://doi.org/10.2147/IJN.S188984>
5. Baumann, M., Krause, M., Overgaard, J., Debus, J., Bentzen, S.M., Daartz, J., Richter, C., Zips, D., Bortfeld, T., 2016. Radiation oncology in the era of precision medicine. *Nat. Rev. Cancer* 16, 234–249. <https://doi.org/10.1038/nrc.2016.18>
6. Bayda, S., Adeel, M., Tuccinardi, T., Cordani, M., Rizzolio, F., 2019. The History of Nanoscience and Nanotechnology: From Chemical-Physical Applications to Nanomedicine. *Mol. Basel Switz.* 25, 112. <https://doi.org/10.3390/molecules25010112>
7. Bertolucci, E., Galletti, A., Antonetti, C., Marracci, M., Tellini, B., Piccinelli, F., Visone, C., 2015. Chemical and magnetic properties characterization of magnetic nanoparticles. *Conf. Rec. - IEEE*

- Instrum. Meas. Technol. Conf. 2015, 1492–1496.
<https://doi.org/10.1109/I2MTC.2015.7151498>
8. Blackadar, C.B., 2016. Historical review of the causes of cancer. *World J. Clin. Oncol.* 7, 54–86.
<https://doi.org/10.5306/wjco.v7.i1.54>
 9. Butterfly, B., 2019. FTIR: Fourier-Transform Infrared Spectroscopy Principles and Applications [WWW Document]. FindLight Blog. URL <https://www.findlight.net/blog/ftir-principles-applications/> (accessed 4.15.23).
 10. Castano, A.P., Demidova, T.N., Hamblin, M.R., 2004. Mechanisms in photodynamic therapy: part one—photosensitizers, photochemistry and cellular localization. *Photodiagnosis Photodyn. Ther.* 1, 279–293. [https://doi.org/10.1016/S1572-1000\(05\)00007-4](https://doi.org/10.1016/S1572-1000(05)00007-4)
 11. Catalano, E., 2016. Role of phytochemicals in the chemoprevention of tumors.
<https://doi.org/10.48550/arXiv.1605.04519>
 12. Chaudhari, V.S., Gawali, B., Saha, P., Naidu, V.G.M., Murty, U.S., Banerjee, S., 2021. Quercetin and piperine enriched nanostructured lipid carriers (NLCs) to improve apoptosis in oral squamous cellular carcinoma (FaDu cells) with improved biodistribution profile. *Eur. J. Pharmacol.* 909, 174400.
 13. Dougherty, T.J., Gomer, C.J., Henderson, B.W., Jori, G., Kessel, D., Korbelik, M., Moan, J., Peng, Q., 1998. Photodynamic Therapy. *J. Natl. Cancer Inst.* 90.
 14. Gharat, S.A., Momin, M., Bhavsar, C., 2016. Oral Squamous Cell Carcinoma: Current Treatment Strategies and Nanotechnology-Based Approaches for Prevention and Therapy. *Crit. Rev. Ther. Drug Carrier Syst.* 33, 363–400.
<https://doi.org/10.1615/CritRevTherDrugCarrierSyst.2016016272>

15. Henderson, B.W., Dougherty, T.J., 1992. How does photodynamic therapy work? *Photochem. Photobiol.* 55, 145–157.
16. Hertzberg, R.P., Caranfa, M.J., Holden, K.G., Jakas, D.R., Gallagher, G., Mattern, M.R., Mong, S.M., Bartus, J.O., Johnson, R.K., Kingsbury, W.D., 1989. Modification of the hydroxylactone ring of camptothecin: inhibition of mammalian topoisomerase I and biological activity. *J. Med. Chem.* 32, 715–720.
17. Ibarra, J., Melendres, J., Almada, M., Burboa, M.G., Taboada, P., Juárez, J., Valdez, M.A., 2015. Synthesis and characterization of magnetite/PLGA/chitosan nanoparticles. *Mater. Res. Express* 2, 095010.
18. Imam, S.S., Alshehi, S., Altamimi, M.A., Hussain, A., Qamar, W., Gilani, S.J., Zafar, A., Alruwaili, N.K., Alanazi, S., Almutairy, B.K., 2021. Formulation of piperine–chitosan-coated liposomes: characterization and In Vitro Cytotoxic Evaluation. *Molecules* 26, 3281.
19. Josefsen, L.B., Boyle, R.W., 2008. Photodynamic therapy and the development of metal-based photosensitisers. *Met.-Based Drugs* 2008.
20. Joshi, B., Joshi, A., 2022. Polymeric magnetic nanoparticles: a multitargeting approach for brain tumour therapy and imaging. *Drug Deliv. Transl. Res.* 12, 1588–1604. <https://doi.org/10.1007/s13346-021-01063-9>
21. Kaur, J., Singh, R.R., Khan, E., Kumar, A., Joshi, A., 2021. Piperine-Loaded PLGA Nanoparticles as Cancer Drug Carriers. *ACS Appl. Nano Mater.* 4, 14197–14207. <https://doi.org/10.1021/acsanm.1c03664>
22. Khan, A.W., Farooq, M., Haseeb, M., Choi, S., 2022. Role of Plant-Derived Active Constituents in Cancer Treatment and Their Mechanisms of Action. *Cells* 11, 1326. <https://doi.org/10.3390/cells11081326>

23. Khanal, S., Adhikari, U., Rijal, N., Bhattarai, S., Sankar, J., Bhattarai, N., 2016. pH-Responsive PLGA Nanoparticle for Controlled Payload Delivery of Diclofenac Sodium. *J. Funct. Biomater.* 7. <https://doi.org/10.3390/jfb7030021>
24. Landgraf, M., Lah, C.A., Kaur, I., Shafiee, A., Sanchez-Herrero, A., Janowicz, P.W., Ravichandran, A., Howard, C.B., Cifuentes-Rius, A., McGovern, J.A., Voelcker, N.H., Hutmacher, D.W., 2020. Targeted camptothecin delivery via silicon nanoparticles reduces breast cancer metastasis. *Biomaterials* 240, 119791. <https://doi.org/10.1016/j.biomaterials.2020.119791>
25. Martino, E., Della Volpe, S., Terribile, E., Benetti, E., Sakaj, M., Centamore, A., Sala, A., Collina, S., 2017. The long story of camptothecin: From traditional medicine to drugs. *Bioorg. Med. Chem. Lett.* 27, 701–707. <https://doi.org/10.1016/j.bmcl.2016.12.085>
26. McCarron, P.A., Marouf, W.M., Quinn, D.J., Fay, F., Burden, R.E., Olwill, S.A., Scott, C.J., 2008. Antibody Targeting of Camptothecin-Loaded PLGA Nanoparticles to Tumor Cells. *Bioconjug. Chem.* 19, 1561–1569. <https://doi.org/10.1021/bc800057g>
27. Mir, M., Ahmed, N., Rehman, A. ur, 2017. Recent applications of PLGA based nanostructures in drug delivery. *Colloids Surf. B Biointerfaces* 159, 217–231. <https://doi.org/10.1016/j.colsurfb.2017.07.038>
28. Mohapatra, J., Nigam, S., George, J., Arellano, A.C., Wang, P., Liu, J.P., 2023. Principles and applications of magnetic nanomaterials in magnetically guided bioimaging. *Mater. Today Phys.* 101003.
29. Mu, W., Chu, Q., Liu, Y., Zhang, N., 2020. A Review on Nano-Based Drug Delivery System for Cancer Chemoimmunotherapy.

- Nano-Micro Lett. 12, 142. <https://doi.org/10.1007/s40820-020-00482-6>
30. Palanisamy, S., Wang, Y.-M., 2019. Superparamagnetic iron oxide nanoparticulate system: synthesis, targeting, drug delivery and therapy in cancer. *Dalton Trans.* 48, 9490–9515.
 31. Pizzolato, J.F., Saltz, L.B., 2003. The camptothecins. *The Lancet* 361, 2235–2242.
 32. Rezvantalab, S., Drude, N.I., Moraveji, M.K., Güvener, N., Koons, E.K., Shi, Y., Lammers, T., Kiessling, F., 2018. PLGA-Based Nanoparticles in Cancer Treatment. *Front. Pharmacol.* 9, 1260. <https://doi.org/10.3389/fphar.2018.01260>
 33. Salsabila, H., Fitriani, L., Zaini, E., 2021. RECENT STRATEGIES FOR IMPROVING SOLUBILITY AND ORAL BIOAVAILABILITY OF PIPERINE. *Int. J. Appl. Pharm.* 31–39. <https://doi.org/10.22159/ijap.2021v13i4.41596>
 34. Siddiqui, S., Ahamad, M.S., Jafri, A., Afzal, M., Arshad, M., 2017. Piperine Triggers Apoptosis of Human Oral Squamous Carcinoma Though Cell Cycle Arrest and Mitochondrial Oxidative Stress. *Nutr. Cancer* 69, 791–799. <https://doi.org/10.1080/01635581.2017.1310260>
 35. Sodipo, B., Abdul Aziz, A., 2014. Superparamagnetic iron oxide nanoparticles incorporated into silica nanoparticles by inelastic collision via ultrasonic field: Role of colloidal stability. <https://doi.org/10.1063/1.4915209>
 36. Stojanović-Radić, Z., Pejčić, M., Dimitrijević, M., Aleksić, A., V. Anil Kumar, N., Salehi, B., C. Cho, W., Sharifi-Rad, J., 2019. Piperine-a major principle of black pepper: a review of its bioactivity and studies. *Appl. Sci.* 9, 4270.
 37. WHO, 2018. Latest global cancer data.
 38. Yaffe, P.B., Power Coombs, M.R., Doucette, C.D., Walsh, M., Hoskin, D.W., 2015. Piperine, an alkaloid from black pepper,

- inhibits growth of human colon cancer cells via G1 arrest and apoptosis triggered by endoplasmic reticulum stress. *Mol. Carcinog.* 54, 1070–1085. <https://doi.org/10.1002/mc.22176>
39. Yan Lee, P., K.Y. Wong, K., 2011. Nanomedicine: A New Frontier in Cancer Therapeutics. *Curr. Drug Deliv.* 8, 245–253. <https://doi.org/10.2174/156720111795256110>
40. Yaraswi, P.S., Shetty, K., Yadav, K.S., 2021. Temozolomide nano enabled medicine: promises made by the nanocarriers in glioblastoma therapy. *J. Controlled Release* 336, 549–571. <https://doi.org/10.1016/j.jconrel.2021.07.003>
41. Zhang, M., Liang, J., Yang, Y., Liang, H., Jia, H., Li, D., 2020. Current Trends of Targeted Drug Delivery for Oral Cancer Therapy. *Front. Bioeng. Biotechnol.* 8, 618931. <https://doi.org/10.3389/fbioe.2020.618931>
42. Zhang, M., Liu, E., Cui, Y., Huang, Y., 2017. Nanotechnology-based combination therapy for overcoming multidrug-resistant cancer. *Cancer Biol. Med.* 14, 212. <https://doi.org/10.20892/j.issn.2095-3941.2017.0054>
43. Zürich, Jk., Webdesign Basel &., n.d. LS Instruments | Dynamic Light Scattering DLS [WWW Document]. URL <https://lsinstruments.ch/en/theory/dynamic-light-scattering-dls/introduction> (accessed 4.7.23).